Composite Structures 184 (2018) 613–632

Contents lists available at ScienceDirect

Composite Structures

journal homepage: www.elsevier.com/locate/compstruct

Nonlinear vibrations and energy exchange of single-walled carbon nanotubes. Radial breathing modes

Matteo Strozzi[a,*], Valeri V. Smirnov[b], Leonid I. Manevitch[b], Francesco Pellicano[c]

[a] Department of Industrial Engineering, University of Bologna, Viale del Risorgimento 2, 40136 Bologna, Italy
[b] N.N. Semenov Institute of Chemical Physics, Russian Academy of Sciences RAS, Ulica Kosygina 4, 119991 Moscow, Russia
[c] Department of Engineering "Enzo Ferrari", University of Modena and Reggio Emilia, Via Pietro Vivarelli 10/1, 41125 Modena, Italy

ARTICLE INFO

Keywords:
Carbon nanotubes
Nonlinear vibrations
Energy beating
Radial breathing modes

ABSTRACT

In this paper, the nonlinear vibrations and energy exchange of single-walled carbon nanotubes (SWNTs) are analysed. The Sanders-Koiter shell theory is used to model the nonlinear dynamics of the system in the case of finite amplitude of vibration. The SWNT deformation is described in terms of longitudinal, circumferential and radial displacement fields. Simply supported, clamped and free boundary conditions are applied. The resonant interaction between radial breathing (axisymmetric) modes (RBMs) is analysed. An energy method, based on the Lagrange equations, is considered in order to reduce the nonlinear partial differential equations of motion to a set of nonlinear ordinary differential equations, which is then solved applying the implicit Runge-Kutta numerical method. The present model is validated in linear field comparing the RBM natural frequencies numerically predicted with data reported in the literature from experiments and molecular dynamics simulations. The nonlinear energy exchange between the two halves along the SWNT axis in the time is studied for different amplitudes of initial excitation applied to the two lowest frequency resonant RBMs. The influence of the SWNT aspect ratio on the numerical value of the nonlinear energy beating period under different boundary conditions is analysed.

1. Introduction

Carbon nanotubes (CNTs) were first discovered in 1991 inside the NEC Corporation laboratories by S. Iijima [1], who studied the synthesis of fullerenes and prepared a new type of carbon structures, the CNTs, described as "helical microtubules of graphitic carbon".

Since CNTs present very high Young's modulus (1–2 TPa) and tensile strength (100 GPa), together with very small diameter (1–2 nm), then they can reach natural frequencies of the THz order and can be used as advanced resonators: the small size and high stiffness amplify the resonant frequency of a nano-resonator, improving therefore its sensitivity [2–4].

Starting from their high mechanical and physical properties, CNTs are used as ultrahigh frequency nano-mechanical resonators in a large number of nano-electro-mechanical devices such as sensors, oscillators, charge detectors and field emission devices [5–7]; moreover, the extremely high thermal conductivity of CNTs makes them promising candidates for advanced applications including power electronics, electric motors and generators, heat exchangers [8,9].

CNTs are divided into two classes: single-walled carbon nanotubes (SWNTs), given by a graphene sheet rolled into a cylinder, and multi-walled carbon nanotubes (MWNTs), composed by concentric SWNTs, where the different layers are connected by van der Waals interaction forces.

In the present paper, we are going to analyse nonlinear vibrations and energy exchange between the two halves along the SWNT axis caused by the resonant interaction between radial breathing modes (RBMs), where the energy transfer denotes a strongly non-stationary dynamic process [10].

RBMs correspond to axisymmetric vibrational modes, where the radial displacement is independent of the circumferential coordinate (no circumferential waves) but it is dependent of the longitudinal coordinate along the SWNT axis; moreover, for the RBMs, the bending stiffness is not present since their vibration does not involve bending deformation.

In order to study the RBMs, different approaches were investigated; a large number of experiments, molecular dynamics simulations and equivalent continuum models was conducted.

Resonant Raman spectroscopy (RRS) is an experimental technique which allows the determination of the atomic configuration of the

* Corresponding author.
E-mail address: matteo.strozzi2@unibo.it (M. Strozzi).

http://dx.doi.org/10.1016/j.compstruct.2017.09.108
Received 3 July 2017; Received in revised form 7 September 2017; Accepted 28 September 2017
Available online 06 October 2017

SWNTs, i.e. their chirality indices, and the measure of the natural frequencies of the RBMs by exerting a laser excitation with wavelengths in the range of nanometers and detecting the frequency of the Raman peaks obtained, which correspond to the RBM vibrations, by means of high resolution transmission electron microscopes (TEMs) [11–13].

Molecular dynamics simulations (MDS) provide accurate predictions of RBM natural frequencies for SWNTs with different chiralities, geometries and boundary conditions under external forces, by taking into account atomic structure and interaction potential energy of the carbon atoms associated with bond stretching, torsion and angle changes between adjacent bonds, electrostatic interactions, coupling among different deformations and transverse inertia forces [14–17].

The analogies between the continuous shells and the discrete CNTs led to very large application of the elastic shell theories, as equivalent continuum models, for the study of natural frequencies and mode shapes of the RBMs in CNTs.

Eisenberger et al. [18] analysed the effect of the van der Waals interactions on the vibrations of MWNTs. An elastic multiple thin shell model was used. Based on the Donnell thin shell theory, the RBM natural frequencies of MWNTs with various radii and number of tubes were found.

Elishakoff and Pentaras [19] evaluated the RBM natural frequencies of double-walled CNTs under various boundary conditions considering the Donnell shallow shell theory. They used the Bubnov-Galerkin and Petrov-Galerkin approximate methods to derive the natural frequencies.

Liew and Wang [20] investigated the wave propagation and RBMs natural frequencies in SWNTs via two different elastic shell theories, i.e., Love's thin cylindrical shell theory and Cooper-Naghdi thick cylindrical shell theory, the last one taking into account also the shear and inertia effects.

Silvestre et al. [21] studied the buckling behaviour of SWNTs comparing the Donnell shallow shell and Sanders-Koiter thin shell theory. They demonstrated the inability of the Donnell theory and the validity of the Sanders-Koiter theory in reproducing buckling strains and mode shapes of RBMs.

Strozzi et al. [22] analysed the linear vibrations of SWNTs under various boundary conditions in the framework of the Sanders-Koiter shell theory. They proposed two analytical and numerical models to obtain natural frequencies and mode shapes of RBMs by varying aspect ratio and chirality.

Other relevant studies on the application of the continuous elastic shell theories for the study of the linear and nonlinear vibrations of CNTs can be found in Refs. [23–28].

Readers interested in deepening the knowledge on the shell behaviour are suggested to refer to the fundamental works of Leissa [29] and Yamaki [30]. The first one is mainly focused on dynamics of shells exhibiting different topologies, materials and boundary conditions; the second one is related on buckling and post-buckling of shells in linear and nonlinear fields.

1.1. Present study

In the present paper, the nonlinear vibrations and energy exchange of SWNTs are investigated. The SWNT dynamics is studied within the framework of the Sanders-Koiter shell theory. The RBMs are considered. The SWNT deformation is described in terms of longitudinal, circumferential and radial displacement fields. Simply supported, clamped and free boundary conditions are applied. The three displacement fields are expanded in the nonlinear field by using approximate linear eigenfunctions. An energy method based on the Lagrange equations is used in order to reduce the nonlinear partial differential equations of motion to a set of nonlinear ordinary differential equations, which is solved applying the implicit Runge-Kutta numerical method. The present study is validated in linear field by comparing the natural frequencies of the RBMs obtained with data available in literature from experiments and molecular dynamics simulations. The energy exchange between the two halves along the SWNT axis in the nonlinear field is investigated; different initial excitation amplitudes are imposed to the two lowest frequency resonant RBMs. A nonlinear convergence analysis is made to select the axisymmetric and asymmetric modes in addition to the two lowest frequency resonant RBMs describing an accurate behaviour in nonlinear field; several modal expansions and boundary conditions are studied. The effect of the aspect ratio on the nonlinear energy beating period between the two lowest frequency resonant RBMs under different boundary conditions is evaluated

1.2. Differences between present paper and previous research efforts of the same authors

It is important to underline that the present paper, focused on the nonlinear vibrations of the RBMs, is strictly connected to a paper previously written by the same authors on the nonlinear vibrations of the circumferential flexural modes (CFMs) [26].

In both the papers, the authors investigate the nonlinear dynamics and energy exchange of SWNTs by applying the Sanders-Koiter nonlinear shell theory and considering a numerical solution method.

Again, in both the papers, different values of initial excitation amplitude are imposed to resonant modes and the transition from energy beating to energy localization in nonlinear field is studied.

In Ref. [26], where initial excitation amplitudes were imposed to the two lowest frequency resonant CFMs, it was found that, in the case of small amplitude initial energy, a periodic energy exchange between the two halves of the nanotube takes place. On the other hand, the nonlinear oscillations of the SWNT become localized when the initial excitation intensity exceeds an energy threshold which depends on the length of the SWNT: the amplitude of the smallest initial excitation, corresponding to the energy confinement in one half of the CNT axis, was called *energy localization threshold*.

In the present paper, the authors propose to apply the same procedure of Ref. [26] to the RBMs: by imposing different initial excitation amplitudes on the two lowest frequency resonant RBMs, they want to investigate if the nonlinear oscillations of the SWNT become localized, and if the nonlinear energy localization phenomenon in only one half of the carbon nanotube axis is present also in the case of resonant RBMs.

2. Sanders-Koiter shell theory

In Fig. 1, a circular cylindrical shell having radius R, length L and thickness h is represented; a cylindrical coordinate system $(O; x, \theta, z)$ is considered where the origin O of the reference system is located at the centre of one end of the shell. In Fig. 1, three displacement fields are represented: longitudinal $u\,(x, \theta, t)$, circumferential $v\,(x, \theta, t)$ and radial $w\,(x, \theta, t)$; the radial displacement field w is considered positive outward; (x, θ) are the longitudinal and angular coordinates of an arbitrary point on the middle surface of the shell; z is the radial coordinate along the thickness h; t is the time.

2.1. Displacement fields

The nondimensional displacement fields $(\widetilde{u},\widetilde{v},\widetilde{w})$ can be written in the following form [22]

$$\widetilde{u} = \frac{u}{R} \qquad \widetilde{v} = \frac{v}{R} \qquad \widetilde{w} = \frac{w}{R} \tag{1}$$

where (u, v, w) are the dimensional displacement fields and R is the radius of the carbon nanotube.

2.2. Strain-displacement relationships

The nondimensional middle surface strains of the shell $(\widetilde{\varepsilon}_{x,0},\widetilde{\varepsilon}_{\theta,0},\widetilde{\gamma}_{x\theta,0})$, containing both linear and nonlinear terms, are expressed as [26]

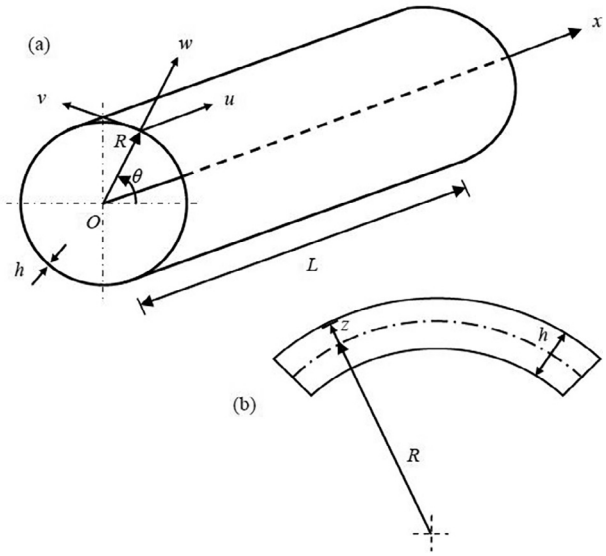

Fig. 1. Geometry of the circular cylindrical shell. (a) Complete shell; (b) cross-section of the shell surface.

$$\widetilde{\varepsilon}_{x,0} = \alpha\frac{\partial\widetilde{u}}{\partial\eta} + \frac{1}{2}\alpha^2\left(\frac{\partial\widetilde{w}}{\partial\eta}\right)^2 + \frac{1}{8}\left(\alpha\frac{\partial\widetilde{v}}{\partial\eta} - \frac{\partial\widetilde{u}}{\partial\theta}\right)^2 \tag{2}$$

$$\widetilde{\varepsilon}_{\theta,0} = \frac{\partial\widetilde{v}}{\partial\theta} + \widetilde{w} + \frac{1}{2}\left(\frac{\partial\widetilde{w}}{\partial\theta} - \widetilde{v}\right)^2 + \frac{1}{8}\left(\frac{\partial\widetilde{u}}{\partial\theta} - \alpha\frac{\partial\widetilde{v}}{\partial\eta}\right)^2 \tag{3}$$

$$\widetilde{\gamma}_{x\theta,0} = \frac{\partial\widetilde{u}}{\partial\theta} + \alpha\frac{\partial\widetilde{v}}{\partial\eta} + \alpha\frac{\partial\widetilde{w}}{\partial\eta}\left(\frac{\partial\widetilde{w}}{\partial\theta} - \widetilde{v}\right) \tag{4}$$

where $\eta = x/L$ is the nondimensional longitudinal coordinate and $\alpha = R/L$.

The nondimensional middle surface changes in curvature and torsion $(\widetilde{k}_x, \widetilde{k}_\theta, \widetilde{k}_{x\theta})$ are given by [22]

$$\begin{aligned}
\widetilde{k}_x &= -\alpha^2\frac{\partial^2\widetilde{w}}{\partial\eta^2} \\
\widetilde{k}_\theta &= \frac{\partial\widetilde{v}}{\partial\theta} - \frac{\partial^2\widetilde{w}}{\partial\theta^2} \\
\widetilde{k}_{x\theta} &= -2\alpha\frac{\partial^2\widetilde{w}}{\partial\eta\partial\theta} + \frac{3}{2}\alpha\frac{\partial\widetilde{v}}{\partial\eta} - \frac{1}{2}\frac{\partial\widetilde{u}}{\partial\theta}
\end{aligned} \tag{5}$$

2.3. Force and moment resultants

The nondimensional force $(\widetilde{N}_x, \widetilde{N}_\theta, \widetilde{N}_{x\theta}, \widetilde{Q}_x, \widetilde{Q}_\theta)$ and moment $(\widetilde{M}_x, \widetilde{M}_\theta, \widetilde{M}_{x\theta})$ resultants of the shell per unit length are given by [22]

$$\begin{aligned}
&\widetilde{N}_x = \widetilde{\varepsilon}_{x,0} + \nu\widetilde{\varepsilon}_{\theta,0} \qquad \widetilde{N}_\theta = \widetilde{\varepsilon}_{\theta,0} + \nu\widetilde{\varepsilon}_{x,0} \qquad \widetilde{N}_{x\theta} = \frac{(1-\nu)}{2}\widetilde{\gamma}_{x\theta,0} \\
&\widetilde{Q}_x = \alpha(\widetilde{k}_{x,x} + \nu\widetilde{k}_{\theta,x}) + \frac{(1-\nu)}{2}\widetilde{k}_{\theta x,\theta} \qquad \widetilde{Q}_\theta = \alpha\frac{(1-\nu)}{2}\widetilde{k}_{x\theta,x} + \widetilde{k}_{\theta,\theta} + \nu\widetilde{k}_{x,\theta} \\
&\widetilde{M}_x = \widetilde{k}_x + \nu\widetilde{k}_\theta \qquad \widetilde{M}_\theta = \widetilde{k}_\theta + \nu\widetilde{k}_x \qquad \widetilde{M}_{x\theta} = \frac{(1-\nu)}{2}\widetilde{k}_{x\theta}
\end{aligned} \tag{6}$$

2.4. Elastic strain energy

The nondimensional elastic strain energy of a cylindrical shell is expressed as follows [22]

$$\widetilde{E} = \frac{1}{2}\frac{1}{(1-\nu^2)}\left[\int_0^1\int_0^{2\pi}\left(\widetilde{\varepsilon}_{x,0}^2 + \widetilde{\varepsilon}_{\theta,0}^2 + 2\nu\widetilde{\varepsilon}_{x,0}\widetilde{\varepsilon}_{\theta,0} + \frac{(1-\nu)}{2}\widetilde{\gamma}_{x\theta,0}^2\right)d\eta d\theta + \frac{\beta^2}{12}\int_0^1\int_0^{2\pi}(\widetilde{k}_x^2 + \widetilde{k}_\theta^2 + 2\nu\widetilde{k}_x\widetilde{k}_\theta + \frac{(1-\nu)}{2}\widetilde{k}_{x\theta}^2)d\eta d\theta\right] \tag{7}$$

where $\beta = h/R$.

2.5. Kinetic energy

The nondimensional time variable τ can be defined by introducing a reference circular frequency ω_0 in the following form [22]

$$\tau = \omega_0 t \qquad \omega_0 = \sqrt{\frac{E}{(1-\nu^2)\rho R^2}} \tag{8}$$

where t is the dimensional time variable and (E, ν, ρ) are the Young's modulus, Poisson's ratio and mass density of the cylindrical shell.

The nondimensional velocity fields $(\widetilde{u}', \widetilde{v}', \widetilde{w}')$ can be obtained from the dimensional displacement fields $(\widetilde{u}, \widetilde{v}, \widetilde{w})$ and the nondimensional time τ in the following form [22]

$$\begin{aligned}
\widetilde{u}' &= \frac{d\widetilde{u}}{d\tau} = \frac{\dot{u}}{R\omega_0} \\
\widetilde{v}' &= \frac{d\widetilde{v}}{d\tau} = \frac{\dot{v}}{R\omega_0} \\
\widetilde{w}' &= \frac{d\widetilde{w}}{d\tau} = \frac{\dot{w}}{R\omega_0}
\end{aligned} \tag{9}$$

where $(\dot{u}, \dot{v}, \dot{w})$ are the dimensional velocity fields.

The nondimensional kinetic energy of a cylindrical shell is given in the following form [22]

$$\widetilde{T} = \frac{1}{2}\gamma\int_0^1\int_0^{2\pi}(\widetilde{u}^{'2} + \widetilde{v}^{'2} + \widetilde{w}^{'2})d\eta d\theta \tag{10}$$

where $\gamma = \rho R^2\omega_0^2/E$.

3. Numerical solution of the Sanders-Koiter shell theory

In order to carry out the numerical analysis of the CNT dynamics, a two-step procedure is applied: (i) the three displacement fields are expanded using a double mixed series, then the Rayleigh-Ritz method is applied to the linear formulation of the problem, in order to obtain an approximation of the eigenfunctions; (ii) the displacement fields are re-expanded by using the linear approximated eigenfunctions, the Lagrange equations are then considered in conjunction with the nonlinear elastic strain energy to obtain a set of nonlinear ordinary differential equations of motion, which are solved numerically.

3.1. Linear vibration analysis

In the linear vibration analysis, only the quadratic terms are retained in the nondimensional elastic strain energy (7).

A modal vibration, i.e., a synchronous motion, can be formally written in the form [22]

$$\begin{aligned}
\widetilde{u}(\eta,\theta,\tau) &= \widetilde{U}(\eta,\theta)\widetilde{f}(\tau) \qquad \widetilde{v}(\eta,\theta,\tau) = \widetilde{V}(\eta,\theta)\widetilde{f}(\tau) \qquad \widetilde{w}(\eta,\theta,\tau) \\
&= \widetilde{W}(\eta,\theta)\widetilde{f}(\tau)
\end{aligned} \tag{11}$$

where $\widetilde{U}(\eta,\theta)$, $\widetilde{V}(\eta,\theta)$, $\widetilde{W}(\eta,\theta)$ represent the mode shape and $\widetilde{f}(\tau)$ describes the time law which is supposed to be the same for each displacement field.

The components of the mode shape $(\widetilde{U}, \widetilde{V}, \widetilde{W})$ are expanded by means of a double mixed series: the periodicity of deformation in the circumferential direction suggests the use of harmonic functions $(\cos n\theta, \sin n\theta)$, while Chebyshev polynomials $T_m^*(\eta)$ are considered in the axial direction [22]

$$\begin{aligned}
\widetilde{U}(\eta,\theta) &= \sum_{m=0}^{M_u}\sum_{n=0}^{N}\widetilde{U}_{m,n}T_m^*(\eta)\cos n\theta \\
\widetilde{V}(\eta,\theta) &= \sum_{m=0}^{M_v}\sum_{n=0}^{N}\widetilde{V}_{m,n}T_m^*(\eta)\sin n\theta \\
\widetilde{W}(\eta,\theta) &= \sum_{m=0}^{M_w}\sum_{n=0}^{N}\widetilde{W}_{m,n}T_m^*(\eta)\cos n\theta
\end{aligned} \tag{12}$$

where $T_m^*(\eta) = T_m(2\eta - 1)$, m is the order of the Chebyshev orthogonal

polynomials, n is the number of nodal diameters and $(\widetilde{U}_{m,n},\widetilde{V}_{m,n},\widetilde{W}_{m,n})$ are the generalized coordinates.

In the specific case of Radial Breathing Modes ($n = 0$), the previous expansions assume the form

$$\begin{aligned}\widetilde{U}(\eta,\theta) &= \sum_{m=0}^{M_u} \widetilde{U}_{m,0} T_m^*(\eta)\\ \widetilde{V}(\eta,\theta) &= \sum_{m=0}^{M_v} \widetilde{V}_{m,0} T_m^*(\eta)\\ \widetilde{W}(\eta,\theta) &= \sum_{m=0}^{M_w} \widetilde{W}_{m,0} T_m^*(\eta)\end{aligned} \tag{13}$$

where these expansions are valid for any value of the circumferential coordinate θ.

3.2. Boundary conditions

Simply supported, clamped and free SWNTs are analysed; the boundary conditions are imposed by applying constraints to the unknown coefficients $(\widetilde{U}_{m,n},\widetilde{V}_{m,n},\widetilde{W}_{m,n})$ of the expansions (12).

3.2.1. Simply supported edges

Simply supported boundary conditions are given by [22]

$$\widetilde{w} = 0 \quad \widetilde{v} = 0 \quad \widetilde{M}_x = 0 \quad \widetilde{N}_x = 0 \quad \eta = 0,1 \tag{14}$$

The previous conditions (14) applied to the expansions (12), considering the nondimensional force and moment resultants (6), imply the following equations [22]

$$\begin{aligned}\widetilde{W}(\eta,\theta) &= \sum_{m=0}^{M_w}\sum_{n=0}^{N} \widetilde{W}_{m,n} T_m^*(\eta)\cos n\theta = 0 \qquad \eta = 0,1\\ \widetilde{V}(\eta,\theta) &= \sum_{m=0}^{M_v}\sum_{n=0}^{N} \widetilde{V}_{m,n} T_m^*(\eta)\sin n\theta = 0 \qquad \eta = 0,1\\ \widetilde{W}_{,\eta\eta}(\eta,\theta) &= \sum_{m=0}^{M_w}\sum_{n=0}^{N} \widetilde{W}_{m,n} T_{m,\eta\eta}^*(\eta)\cos n\theta = 0 \qquad \eta = 0,1\\ \widetilde{U}_{,\eta}(\eta,\theta) &= \sum_{m=0}^{M_u}\sum_{n=0}^{N} \widetilde{U}_{m,n} T_{m,\eta}^*(\eta)\cos n\theta = 0 \qquad \eta = 0,1\end{aligned} \tag{15}$$

where $(\cdot)_{,\eta} = \partial(\cdot)/\partial\eta$ and $(\cdot)_{,\eta\eta} = \partial^2(\cdot)/\partial\eta^2$.

The linear system given by the Eq. (15) can be solved analytically in terms of the coefficients $(\widetilde{U}_{1,n},\widetilde{U}_{2,n},\widetilde{V}_{0,n},\widetilde{V}_{1,n},\widetilde{W}_{0,n},\widetilde{W}_{1,n},\widetilde{W}_{2,n},\widetilde{W}_{3,n})$, since these coefficients are linearly dependent.

3.2.2. Clamped edges

Clamped boundary conditions are given by [22]

$$\widetilde{u} = 0 \qquad \widetilde{v} = 0 \qquad \widetilde{w} = 0 \qquad \widetilde{w}_{,\eta} = 0 \qquad \eta = 0,1 \tag{16}$$

The previous conditions (16) applied to the expansions (12) imply the following equations [22]

$$\begin{aligned}\widetilde{U}(\eta,\theta) &= \sum_{m=0}^{M_u}\sum_{n=0}^{N} \widetilde{U}_{m,n} T_m^*(\eta)\cos n\theta = 0 \quad \eta = 0,1\\ \widetilde{V}(\eta,\theta) &= \sum_{m=0}^{M_v}\sum_{n=0}^{N} \widetilde{V}_{m,n} T_m^*(\eta)\sin n\theta = 0 \quad \eta = 0,1\\ \widetilde{W}(\eta,\theta) &= \sum_{m=0}^{M_w}\sum_{n=0}^{N} \widetilde{W}_{m,n} T_m^*(\eta)\cos n\theta = 0 \quad \eta = 0,1\\ \widetilde{W}_{,\eta}(\eta,\theta) &= \sum_{m=0}^{M_w}\sum_{n=0}^{N} \widetilde{W}_{m,n} T_{m,\eta}^*(\eta)\cos n\theta = 0 \quad \eta = 0,1\end{aligned} \tag{17}$$

where $(\cdot)_{,\eta} = \partial(\cdot)/\partial\eta$.

The linear system given by the equations (17) can be solved analytically in terms of the coefficients $(\widetilde{U}_{0,n},\widetilde{U}_{1,n},\widetilde{V}_{0,n},\widetilde{V}_{1,n},\widetilde{W}_{0,n},\widetilde{W}_{1,n},\widetilde{W}_{2,n},\widetilde{W}_{3,n})$, since these coefficients are linearly dependent.

3.2.3. Free edges

Free boundary conditions are given by [22]

$$\widetilde{N}_x = 0 \qquad \widetilde{N}_{x\theta} + \widetilde{M}_{x\theta} = 0 \qquad \widetilde{Q}_x + \frac{\partial \widetilde{M}_{x\theta}}{\partial\theta} = 0 \qquad \widetilde{M}_x = 0 \qquad \eta = 0,1 \tag{18}$$

In the case of free edges, the complexity of the boundary conditions makes it difficult to follow the previously mentioned procedure; however, in this specific case, all the boundary conditions (18) are of "natural type", i.e., they involve forces and moments, and not of "geometric type", which involve displacements and rotations. It is well known that the Rayleigh-Ritz procedure can be applied even if the natural boundary conditions are not respected by expansions (12), since they will be satisfied by total energy minimization; therefore, no boundary conditions are imposed for the specific case of free edges.

3.3. Rayleigh-Ritz procedure

The maximum number of variables needed for describing a general vibration mode with n nodal diameters is obtained by the relation $(N_p = M_u + M_v + M_w + 3 - p)$, where $(M_u = M_v = M_w)$ denote the maximum degree of the Chebyshev polynomials and p describes the number of equations for the boundary conditions to be respected.

A specific convergence analysis was carried out to select the degree of the Chebyshev polynomials: degree 11 was found suitably accurate, $(M_u = M_v = M_w = 11)$.

For a multi-mode analysis including different values of nodal diameters n, the number of degrees of freedom of the system is computed by the relation (Nmax = Np × (N + 1)), where N represents the maximum value of the nodal diameters n to be considered.

The Eq. (11) are inserted into the expressions of elastic strain energy (7) and kinetic energy (10) to compute the Rayleigh quotient; after imposing the stationarity to the Rayleigh quotient, one obtains the eigenvalue problem [22]

$$(-\omega^2\widetilde{\mathrm{M}} + \widetilde{\mathrm{K}})\widetilde{\mathrm{q}} = \widetilde{0} \tag{19}$$

which gives approximate natural frequencies (eigenvalues) and modes of vibrations (eigenvectors).

The approximate mode shape corresponding to the j-th mode is given by the Eq. (12), where coefficients $(\widetilde{U}_{m,n},\widetilde{V}_{m,n},\widetilde{W}_{m,n})$ are substituted with $(\widetilde{U}_{m,n}^{(j)},\widetilde{V}_{m,n}^{(j)},\widetilde{W}_{m,n}^{(j)})$, which are the components of the j-th eigenvector $\widetilde{q}_j$ obtained from Eq. (19).

The vector function [22]

$$\widetilde{Q}^{(j)}(\eta,\theta) = \begin{bmatrix}\widetilde{U}^{(j)}(\eta,\theta)\\ \widetilde{V}^{(j)}(\eta,\theta)\\ \widetilde{W}^{(j)}(\eta,\theta)\end{bmatrix} \tag{20}$$

is the approximation of the j-th eigenfunction vector of the original problem (step i of the numerical solution).

3.4. Nonlinear vibration analysis

In the nonlinear analysis, the full expression of the nondimensional elastic strain energy (7), which contains terms up to the fourth order (cubic nonlinearity), is considered.

The three displacement fields $\widetilde{u}(\eta,\theta,\tau)$, $\widetilde{v}(\eta,\theta,\tau)$, $\widetilde{w}(\eta,\theta,\tau)$ are expanded using the approximate mode shapes $\widetilde{U}^{(j,n)}(\eta,\theta)$, $\widetilde{V}^{(j,n)}(\eta,\theta)$, $\widetilde{W}^{(j,n)}(\eta,\theta)$ obtained in the linear analysis, in the form [26]

$$\widetilde{u}(\eta,\theta,\tau) = \sum_{j=1}^{N_u}\sum_{n=1}^{N} \widetilde{U}^{(j,n)}(\eta,\theta)\widetilde{f}_{u,j,n}(\tau)$$
$$\widetilde{v}(\eta,\theta,\tau) = \sum_{j=1}^{N_v}\sum_{n=1}^{N} \widetilde{V}^{(j,n)}(\eta,\theta)\widetilde{f}_{v,j,n}(\tau)$$
$$\widetilde{w}(\eta,\theta,\tau) = \sum_{j=1}^{N_w}\sum_{n=1}^{N} \widetilde{W}^{(j,n)}(\eta,\theta)\widetilde{f}_{w,j,n}(\tau) \tag{21}$$

These expansions respect exactly the boundary conditions; the synchronicity is now relaxed since for each mode j and each component $(\widetilde{u},\widetilde{v},\widetilde{w})$ different time laws $\widetilde{f}(\tau)$ are allowed.

The mode shapes $\widetilde{U}^{(j,n)}(\eta,\theta)$, $\widetilde{V}^{(j,n)}(\eta,\theta)$, $\widetilde{W}^{(j,n)}(\eta,\theta)$ are known functions expressed in terms of polynomials and harmonic functions, see Eq. (12), where the index j is used for ordering the modes with increasing associated natural frequency and the index n indicates the number of nodal diameters; the time laws $(\widetilde{f}_{u,j,n}(\tau),\widetilde{f}_{v,j,n}(\tau),\widetilde{f}_{w,j,n}(\tau))$ are unknown functions.

3.5. Lagrange equations

Expansions (21) are inserted into the expressions of the nondimensional elastic strain energy (7) and kinetic energy (10); then, the nondimensional Lagrange equations of motion for free vibrations can be expressed in the form [26]

$$\frac{d}{d\tau}\left(\frac{\partial\widetilde{T}}{\partial\widetilde{q}_i'}\right) + \frac{\partial\widetilde{E}}{\partial\widetilde{q}_i} = 0 \quad i \in [1,N_{\max}] \tag{22}$$

where the maximum number of degrees of freedom $N_{\max}$ depends on the number of vibration modes considered in the expansions (21).

The nondimensional lagrangian coordinates $(\widetilde{q}_i,\widetilde{q}_i')$ can be written as

$$\widetilde{q}_i = \frac{q_i}{R} \quad \widetilde{q}_i' = \frac{d\widetilde{q}_i}{d\tau} \quad i \in [1,N_{\max}] \tag{23}$$

where the nondimensional lagrangian coordinates $\widetilde{q}_i$ correspond to the previous nondimensional modal coordinates $(\widetilde{f}_{u,j,n}(\tau),\widetilde{f}_{v,j,n}(\tau),\widetilde{f}_{w,j,n}(\tau))$.

The nondimensional mass matrix $\widetilde{M}$ is connected to the nondimensional kinetic energy $\widetilde{T}$ by the nondimensional lagrangian coordinate $\widetilde{q}_i''$ in the following form

$$\frac{d}{d\tau}\left(\frac{\partial\widetilde{T}}{\partial\widetilde{q}_i'}\right) = \widetilde{M}\widetilde{q}_i'' \qquad \widetilde{q}_i'' = \frac{d^2\widetilde{q}_i}{d\tau^2} \qquad i \in [1,N_{\max}] \tag{24}$$

The nondimensional vector function $\widetilde{F}(\widetilde{q}_i)$ is connected to the nondimensional potential energy $\widetilde{E}$ in the following form

$$\frac{\partial\widetilde{E}}{\partial\widetilde{q}_i} = \widetilde{F}(\widetilde{q}_i) \quad i \in [1,N_{\max}] \tag{25}$$

By substituting the vector functions $\widetilde{M}\widetilde{q}_i''$ (24) and $\widetilde{F}(\widetilde{q}_i)$ (25) into equation (22), we obtain

$$\widetilde{M}\widetilde{q}_i'' + \widetilde{F}(\widetilde{q}_i) = 0 \quad i \in [1,N_{\max}] \tag{26}$$

Introducing the vector function $\widetilde{F}_{x,i} = \widetilde{M}^{-1}\widetilde{F}(\widetilde{q}_i)$ in the Eq. (26), the nondimensional Lagrange equations of motion for free vibrations can be expressed in the following form

$$\widetilde{q}_i'' + \widetilde{F}_{x,i} = 0 \quad i \in [1,N_{\max}] \tag{27}$$

Using the Lagrange Eq. (27), a set of nonlinear ordinary differential equations is obtained; these equations must be completed with suitable modal initial conditions on the displacements and velocities. This system of nonlinear equations of motion is finally solved using the implicit Runge-Kutta numerical method with suitable accuracy and precision (step ii of the numerical solution).

4. Nonlinear energy exchange along the SWNT axis

In the present section, the nonlinear energy exchange between the two halves along the SWNT axis in the time is investigated. The dynamical system is conservative (no damping). A simply supported SWNT with aspect ratio $L/R = 20$ is considered. As initial condition, a localized energy in only one half of the carbon nanotube is imposed and it is checked if the energy remains localized in the time. Different initial excitation amplitudes are applied on the two lowest frequency resonant RBMs (the higher order axisymmetric and asymmetric modes are not directly excited). The energy beating and localization phenomena are examined. The differences between the present case (resonant RBMs) and the case previously studied by the same Authors in Ref. [26] (resonant CFMs) are highlighted.

In the case of small amplitude initial excitation, a weak resonant interaction between the two RBMs takes place, the initial localized energy (as initial condition) is immediately destroyed and a periodic energy exchange between the two halves of the SWNT axis arises. The time scale of this periodic energy redistribution is inversely proportional to the difference of the natural frequencies of the two RBMs. This phenomenon can be interpreted as the energy beating between two effective particles, each one containing about one half of the SWNT axis.

When the amplitude of the initial excitation increases, a strong resonant interaction between the two RBMs takes place and the effect of the nonlinearity increases; again, the initial localized energy is immediately destroyed and a periodic energy exchange between the two halves of the SWNT axis is present, with the same time period of the previous case of small amplitude initial excitation.

It is important to underline that, in case of RBMs (differently from CFMs [26]), the low-frequency nonlinear vibrations do not become localized ones for any amplitude of the initial excitation energy (no energy localization in one half of the SWNT axis), and a periodic energy exchange between the two halves along the axis is always present, where the time period of the nonlinear energy beating is not dependent on the initial excitation amplitude: therefore, in the specific case of RBMs, the nonlinear energy beating is always permitted and no energy localization threshold is present.

In the following section, the energy exchange along the SWNT axis in nonlinear field for the RBMs is investigated by imposing different initial excitation amplitudes.

4.1. Effect of the initial excitation amplitude

By considering the lagrangian coordinates $\widetilde{f}_{j,n}(\tau)$ of the nonlinear expansions (21), and assuming the modal initial conditions $\widetilde{f}_{1,0}(0) = \widetilde{f}_{2,0}(0) = \widetilde{f}(0)$ on the two lowest frequency RBMs (1,0),(2,0) along the displacement fields (u,v,w), the initial excitation amplitude $\widetilde{X}(0)$ can be written as [26]

$$\widetilde{X}(0) = \frac{\widetilde{f}^2(0)}{2\varepsilon^2}(\widetilde{\omega}_1 + \widetilde{\omega}_2) \tag{28}$$

where the small parameter ε gives the relative difference between the two nondimensional circular frequencies $(\widetilde{\omega}_1,\widetilde{\omega}_2)$ of the two lowest frequency RBMs (1,0),(2,0), respectively [26]

$$\varepsilon = \sqrt{\frac{\widetilde{\omega}_2 - \widetilde{\omega}_1}{\widetilde{\omega}_1}} \tag{29}$$

It should be highlighted that, in the present paper, the initial velocities are taken equal to zero (the modal initial conditions are imposed only on the displacements).

In Fig. 2, the time history and evolution of the total energy distribution in time along the axis of a simply supported SWNT with aspect ratio $L/R = 20$ are shown; the numerical method and Eq. (28) are applied; different initial excitation amplitudes are imposed on the two

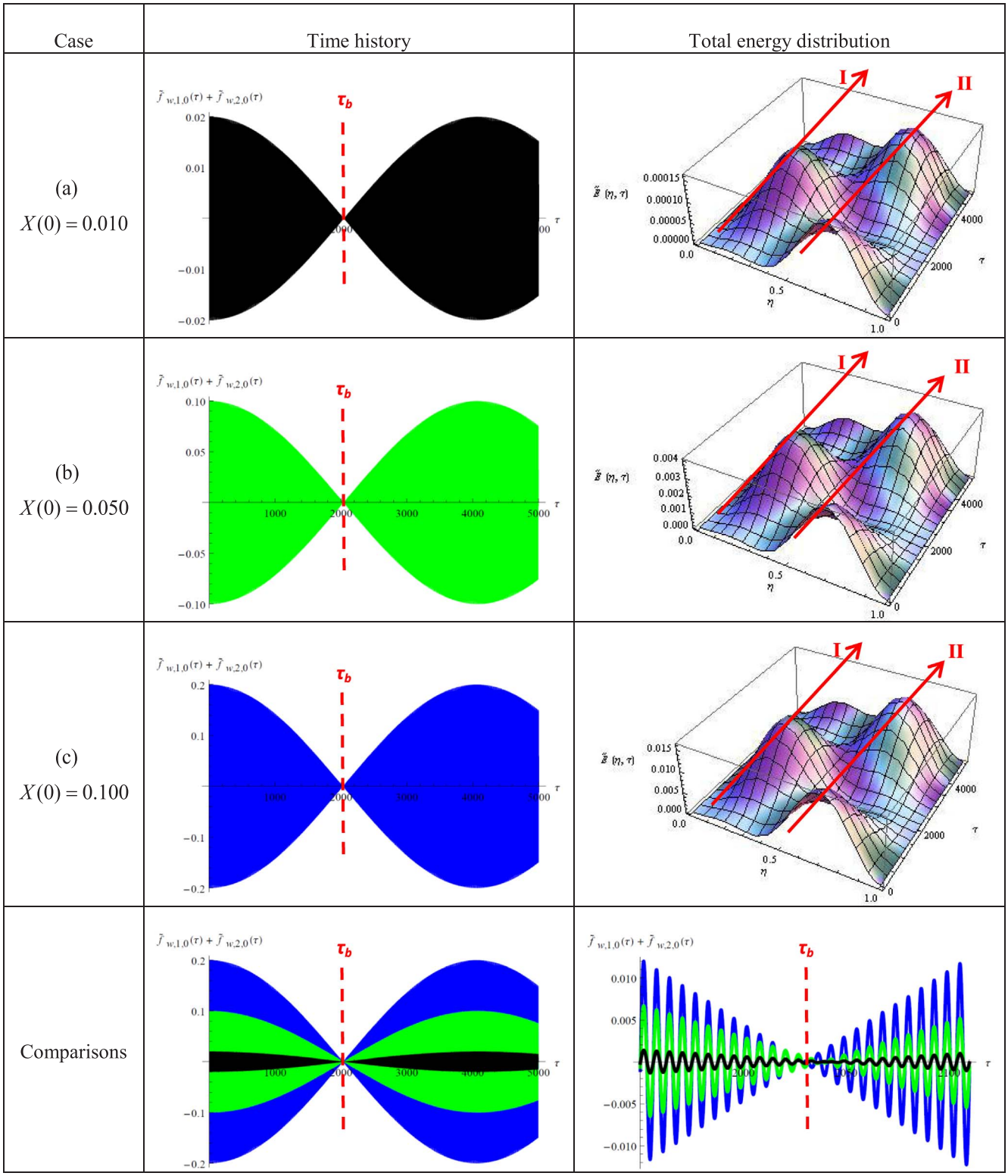

Fig. 2. Time history and evolution of the total energy distribution in time along the axis of a simply supported SWNT with $L/R = 20$; numerical method. (a) Initial excitation amplitude $\widetilde{X}(0) = 0.010$; nonlinear energy beating period $\tau_b = 2030$. (b) Initial excitation amplitude $\widetilde{X}(0) = 0.050$; nonlinear energy beating period $\tau_b = 2030$. (c) Initial excitation amplitude $\widetilde{X}(0) = 0.100$; nonlinear energy beating period $\tau_b = 2030$.

lowest frequency resonant axisymmetric modes (1,0) and (2,0); the initial excitation domain ($\tau = 0$) is always localized in the second half of the SWNT axis ($0.5 \leq \eta \leq 1$) (initial localized energy).

In Fig. 2(a) the very low initial excitation amplitude $\widetilde{X}(0) = 0.010$ is used (very weak resonant interaction between the two RBMs) and a periodic quasi-linear energy exchange between the two halves of the SWNT axis is present (very low peak of total energy distribution): the energy beating period is equal to $\tau_b = 2030$.

In Fig. 2(b) the low initial excitation amplitude $\widetilde{X}(0) = 0.050$ is used (weak resonant interaction between the two RBMs) and a periodic weakly nonlinear energy exchange between the two halves of the SWNT axis is present (low peak of total energy distribution), with the same

Table 1
Mechanical parameters of the SWNT [27,28].

Young's modulus E [TPa]	5.5
Poisson's ratio ν	0.19
Mass density ρ [kg/m^3]	11700
Thickness h [nm]	0.066
Radius R [nm]	0.786

energy beating period of Fig. 2(a).

In Fig. 2(c) the high initial excitation amplitude $\widetilde{X}(0) = 0.100$ is used (strong resonant interaction between the two RBMs) and a periodic strongly nonlinear energy exchange between the two halves of the SWNT axis is present (high peak of total energy distribution), with the same energy beating period of Fig. 2(a) and (b).

From the previous numerical analyses for the RBM nonlinear vibrations, it was found that, for any amplitude of initial excitation, the initial energy localization in the second half of the SWNT axis is promptly lost, and a periodic energy exchange between the two halves of the SWNT axis arises; in addition, the nonlinear energy beating period τ_b is not dependent on the initial excitation amplitude and no energy localization is achieved forever.

5. Numerical results

The mechanical parameters of the zigzag ($r = 20$, $s = 0$) SWNT studied in this paper are listed in Table 1; it must be underlined that the same SWNT (chirality and mechanical parameters) was previously analysed by the same Authors in Refs. [22] (linear vibrations) and [26] (nonlinear CFM vibrations).

In the present section, comparisons between the RBM natural frequencies obtained by applying the Sanders-Koiter shell theory, resonant Raman spectroscopy and molecular dynamics simulations are reported to validate in linear field the continuum approach proposed in this paper.

Then, a convergence analysis is carried out in order to select the higher order axisymmetric and the asymmetric modes providing accurate result in nonlinear field; several nonlinear modal expansions and different boundary conditions are used; a specific aspect ratio and initial excitation amplitude is considered.

At the end, the effect of the SWNT aspect ratio on the value of the nonlinear energy beating period for the resonant RBMs is investigated; a specific initial excitation amplitude and nonlinear modal expansion is considered; different boundary conditions are applied.

5.1. Validation of the numerical approach in linear field

In this section, the numerical approach based on the Sanders-Koiter shell theory proposed in this paper is validated in linear field. The natural frequencies of the RBMs obtained are compared with data available in the pertinent literature from resonant Raman spectroscopy (RRS) experiments and molecular dynamics simulations (MDS).

The comparisons reported in Tables 2 and 3 denote that the present continuum approach, based on the Sanders-Koiter thin shell theory, gives excellent results in terms of natural frequencies; moreover, it is proved that the equivalent mechanical parameters of the SWNT reported in Table 1 are correct.

In particular, the natural frequencies of the RBMs based on the present numerical model are in good agreement with the RRS experimental results. In Table 2, comparisons for several armchair, zigzag and chiral SWNTs with a specific aspect ratio under free-free boundary conditions are reported. The natural frequencies of the first RBM decrease increasing the chirality, i.e., the SWNT diameter. The relative errors between the complete Sanders-Koiter shell theory and the RRS are less than 5%, and it appears a satisfactory accuracy.

Moreover, natural frequencies of RBMs for different armchair and zigzag SWNTs under free-free boundary conditions with different aspect ratios are reported in Table 3. The natural frequencies of the first RBM decrease increasing the chirality, i.e., the SWNT diameter, and increasing the aspect ratio. From these comparisons, it can be seen that the present numerical model based on the Sanders -Koiter shell theory is in good agreement with the MDS of the radial breathing modes, with relative errors less than 4%.

Table 2
Natural frequencies of the first RBM ($j = 0$, $n = 0$). Free-free SWNTs. Chirality (r, s). Aspect ratio L/D. Comparisons between Sanders-Koiter shell theory (SKT) and resonant Raman spectroscopy (RRS).

Natural frequency (THz)				Difference%
(r, s)	L/D	SKT – Present model	RRS – Ref. [12]	
(10,5)	10	6.785	7.105	4.50
(11,4)	10	6.669	6.865	2.85
(9,7)	10	6.461	6.742	4.17
(10,6)	10	6.414	6.688	4.10
(14,1)	10	6.177	6.295	1.87
(18,0)	10	5.025	5.276	4.76
(17,2)	10	4.964	5.216	4.83
(16,4)	10	4.895	5.066	3.37
(15,6)	10	4.788	4.947	3.21
(11,11)	10	4.711	4.917	4.19
(14,8)	10	4.655	4.857	4.16
(19,1)	10	4.594	4.797	4.23
(18,3)	10	4.559	4.737	3.76
(13,10)	10	4.494	4.677	3.91
(17,5)	10	4.494	4.677	3.91
(16,7)	10	4.393	4.617	4.85
(12,12)	10	4.318	4.527	4.62
(15,9)	10	4.276	4.461	4.15
(21,0)	10	4.271	4.437	3.74
(20,2)	10	4.260	4.446	4.18

Table 3
Natural frequencies of the first RBM ($j = 0$, $n = 0$). Free-free SWNTs. Chirality (r, s). Aspect ratio L/D. Comparisons between Sanders-Koiter shell theory (SKT) and molecular dynamics simulations (MDS).

Natural frequency (THz)				Difference %
(r, s)	L/D	SKT – Present model	MDS – Ref. [16]	
(12,0)	5.677	7.478	7.272	2.83
(7,7)	5.577	7.399	7.166	3.25
(9,6)	5.827	6.865	6.649	3.25
(10,5)	5.289	6.785	6.581	3.10
(8,8)	5.673	6.473	6.275	3.15
(14,0)	5.771	6.414	6.235	2.87
(11,7)	5.333	5.715	5.550	2.97
(16,0)	6.070	5.606	5.455	2.77
(10,10)	5.626	5.184	5.026	3.14
(15,4)	5.445	5.176	5.018	2.94
(18,0)	5.598	4.985	4.850	2.78
(20,0)	5.671	4.489	4.364	2.86
(12,12)	5.671	4.318	4.190	3.05
(25,0)	5.624	3.590	3.491	2.84
(15,15)	5.624	3.453	3.354	2.95
(30,0)	5.683	2.991	2.908	2.85
(18,18)	5.644	2.878	2.796	2.93
(33,0)	6.239	2.718	2.623	3.62
(20,20)	5.669	2.590	2.516	2.94
(36,0)	5.669	2.493	2.423	2.89

5.2. Nonlinear convergence analysis

The first step of the nonlinear analysis for the numerical approach is the convergence check in terms of the nonlinear modal expansions (21); it is carried out on the zigzag ($r = 20$, $s = 0$) SWNT of Table 1 with aspect ratio $L/R = 20$ and different boundary conditions in order to

select the correct number and type of vibrating modes which provide an accurate behaviour in nonlinear field.

An initial two-mode approximation involving only the two lowest frequency resonant axisymmetric modes (1,0),(2,0) is considered (4 dof model); the convergence is then checked by adding suitable modes to the two resonant RBM ones, i.e. higher order axisymmetric modes and asymmetric modes (quadratic and cubic nonlinearities); the initial excitation domain ($\tau = 0$) is imposed to be localized in the second half of the SWNT axis ($0.5 \leq \eta \leq 1$).

It is important to underline that the initial excitation amplitude imposed on the two resonant modes (1,0),(2,0), given by $\widetilde{X}(0) = 0.100$, is very high if compared with the initial excitation amplitude imposed on the additional axisymmetric and asymmetric modes, equal to $\widetilde{X}(0) = 0.005$; however, it is proven in this paper that the presence of additional axisymmetric and asymmetric modes in the modal expansions is fundamental to predict the correct nonlinear behaviour of the SWNT: indeed, the fully convergence is reached with a 24 dof model (Tables 4–6) described in the following, which is assumed as a reference, where the energy beating period τ_b is adopted as convergence parameter.

5.2.1. Simply supported boundary conditions

In Table 4 and Fig. 3, the convergence analysis for the numerical method in the case of simply supported boundary conditions is reported. Time histories obtained by considering nonlinear modal expansions with different degrees of freedom are compared for the aspect ratio $L/R = 20$.

The high initial excitation amplitude $\widetilde{X}(0) = 0.100$ is applied (strong resonant interaction between the two lowest frequency RBMs with strongly nonlinear periodic energy exchange between the two halves of the SWNT axis); the nonlinear modal expansion with 24 dof is assumed as the reference one ($\tau_b = 2148$).

From the numerical analyses, it can be found that the 4-10-16-18-24 dof expansions behave quite similarly, and the smallest modal expansion able to predict the nonlinear dynamics of the nanotube with acceptable accuracy (less than 5%) is the 10 dof model ($\Delta\tau_b\% = 3.40$).

It must be underlined that the 4 dof model considered in the present section corresponds to the case reported in Fig. 2(c) (simply supported SWNT, aspect ratio $L/R = 20$, initial excitation amplitude $\widetilde{X}(0) = 0.100$, energy beating period $\tau_b = 2030$), where the initial excitation amplitude was applied only on the two RBMs (1,0),(2,0) (the higher order axisymmetric and asymmetric modes were not directly excited), therefore considering a nonlinear modal expansion with 4 degrees of freedom.

5.2.2. Clamped-clamped boundary conditions

In Table 5 and Fig. 4, the convergence analysis for the numerical method in case of clamped-clamped boundary conditions is reported. Time histories obtained by considering nonlinear modal expansions with different degrees of freedom are compared for the aspect ratio $L/R = 20$.

The high initial excitation amplitude $\widetilde{X}(0) = 0.100$ is applied (strong resonant interaction between the two lowest frequency RBMs with strongly nonlinear periodic energy exchange between the two halves of the SWNT axis); the nonlinear modal expansion with 24 dof is assumed as the reference one ($\tau_b = 1179$).

From the numerical analyses, similarly to the case of simply supported boundary conditions, it can be observed that, also in the case of clamped-clamped edges, the 4-10-16-18-24 dof expansions behave quite similarly, and the smallest modal expansion able to predict the nonlinear dynamics of the carbon nanotube with acceptable accuracy (less than 5%) is the 10 dof model ($\Delta\tau_b\% = 4.76$).

5.2.3. Free-free boundary conditions

In Table 6 and Fig. 5, the convergence analysis for the numerical method in the case of free-free boundary conditions is reported. Time histories obtained considering nonlinear modal expansions with different degrees of freedom are compared for the aspect ratio $L/R = 20$.

The high initial excitation amplitude $\widetilde{X}(0) = 0.100$ is applied (strong resonant interaction between the two lowest frequency RBMs with strongly nonlinear periodic energy exchange between the two halves of the SWNT axis); the nonlinear modal expansion with 24 dof is assumed as the reference one ($\tau_b = 2794$).

From the numerical analyses, similarly to the cases of simply supported and clamped-clamped boundary conditions, it can be found that, also in the case of free-free edges, the 4-10-16-18-24 dof expansions behave quite similarly, and the smallest modal expansion able to predict the nonlinear dynamics of the SWNT with acceptable accuracy (less than 5%) is the 10 dof model ($\Delta\tau_b\% = 4.06$).

5.2.4. Comparisons

From the previous nonlinear convergence analyses performed on the SWNT of Table 1, considering the same aspect ratio $L/R = 20$ and imposing the same initial excitation amplitude $\widetilde{X}(0) = 0.100$, it can be deduced that the 10 dof model (Tables 4–6) provides very satisfactory results with minimal computational effort for all the considered boundary conditions (Figs. 3–5).

The previous considerations suggest that the following 10 dof modal expansion should be used for studying the nonlinear internal resonance of the radial breathing (axisymmetric) modes (1,0), (2,0):

- modes (1,0), (2,0), (1,2), (2,2) for the longitudinal displacement field u
- modes (1,2), (2,2) for the circumferential displacement field v
- modes (1,0), (2,0), (1,2), (2,2) for the radial displacement field w

After selecting these modes the longitudinal and radial nonlinear modal expansions (21) are reduced to a four-term model, while the circumferential nonlinear modal expansion is reduced to a two-term model; the resulting nonlinear modal expansion has therefore a total number of 10 dof.

It must be underlined that the main weakness of the 4 dof model is given by the insufficient number of asymmetric modes, which are important for properly modelling the middle surface deformations of the SWNT, Eqs. (2-5), during the modal vibration.

Moreover, from the previous convergence analyses for the RBM nonlinear vibrations, it was found that, for specific aspect ratio, initial excitation amplitude and modal expansion, the nonlinear energy beating period τ_b depends on the boundary condition applied.

In Fig. 6, the total energy distributions corresponding to the time

Table 4
Convergence analysis. Numerical method. Nonlinear modal expansions. Nonlinear energy beating period τ_b. Reference 24 dof model. Simply supported edges. Aspect ratio $L/R = 20$. Initial excitation amplitude $\widetilde{X}(0) = 0.100$.

(j, n)	(1,0)	(2,0)	(3,0)	(1,2)	(2,2)	(3,2)	(1,4)	(2,4)	(3,4)	τ_b	$\Delta\tau_b\%$
4 dof model	*u, w*	*u, w*	–	–	–	–	–	–	–	2030	5.49
10 dof model	***u, w***	***u, w***	**–**	***u, v, w***	***u, v, w***	**–**	**–**	**–**	**–**	**2075**	**3.40**
16 dof model	*u, w*	*u, w*	–	*u, v, w*	*u, v, w*	–	*u, v, w*	*u, v, w*	–	2099	2.28
18 dof model	*u, w*	*u, w*	*u, w*	*u, v, w*	*u, v, w*	–	*u, v, w*	*u, v, w*	–	2122	1.21
24 dof model	*u, w*	*u, w*	*u, w*	*u, v, w*	*u, v, w*	*u, v, w*	*u, v, w*	*u, v, w*	*u, v, w*	2148	

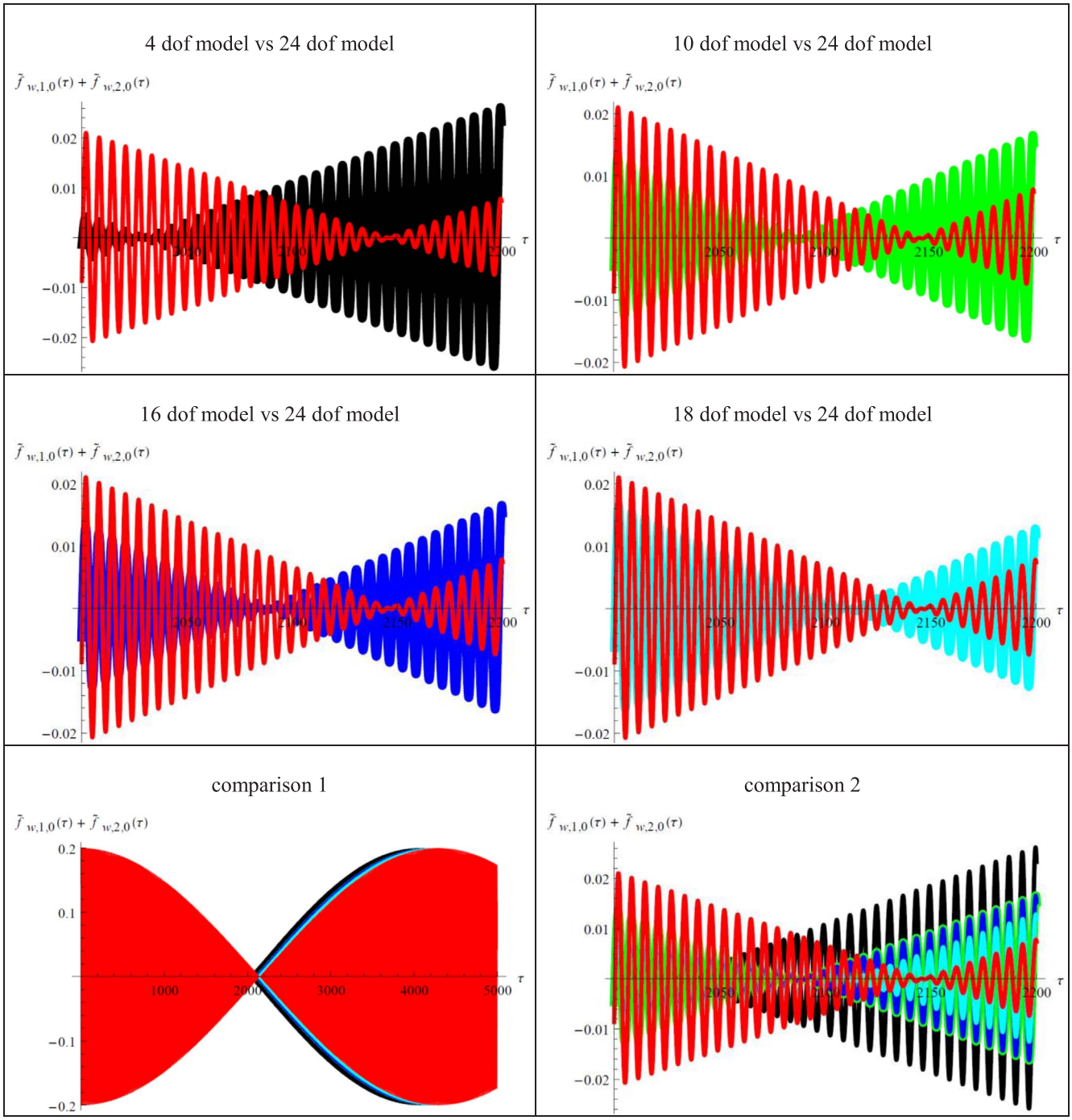

Fig. 3. Convergence analysis. Numerical method. Nonlinear modal expansions. Simply supported edges. $L/R = 20$. Initial amplitude $\widetilde{X}(0) = 0.100$. Time histories. "—", 4 dof. "—", 10 dof. "—", 16 dof. "—", 18 dof. "—", 24 dof.

Table 5
Convergence analysis. Numerical method. Nonlinear modal expansions. Nonlinear energy beating period τ_b. Reference 24 dof model. Clamped-clamped edges. Aspect ratio $L/R = 20$. Initial excitation amplitude $\widetilde{X}(0) = 0.100$.

(j,n)	(1,0)	(2,0)	(3,0)	(1,2)	(2,2)	(3,2)	(1,4)	(2,4)	(3,4)	τ_b	$\Delta\tau_b$%
4 dof model	*u, w*	*u, w*	–	–	–	–	–	–	–	1052	10.8
10 dof model	***u, w***	***u, w***	**–**	***u, v, w***	***u, v, w***	**–**	**–**	**–**	**–**	**1123**	**4.76**
16 dof model	*u, w*	*u, w*	–	*u, v, w*	*u, v, w*	–	*u, v, w*	*u, v, w*	–	1142	3.13
18 dof model	*u, w*	*u, w*	*u, w*	*u, v, w*	*u, v, w*	–	*u, v, w*	*u, v, w*	–	1159	1.68
24 dof model	*u, w*	*u, w*	*u, w*	*u, v, w*	*u, v, w*	*u, v, w*	*u, v, w*	*u, v, w*	*u, v, w*	1179	

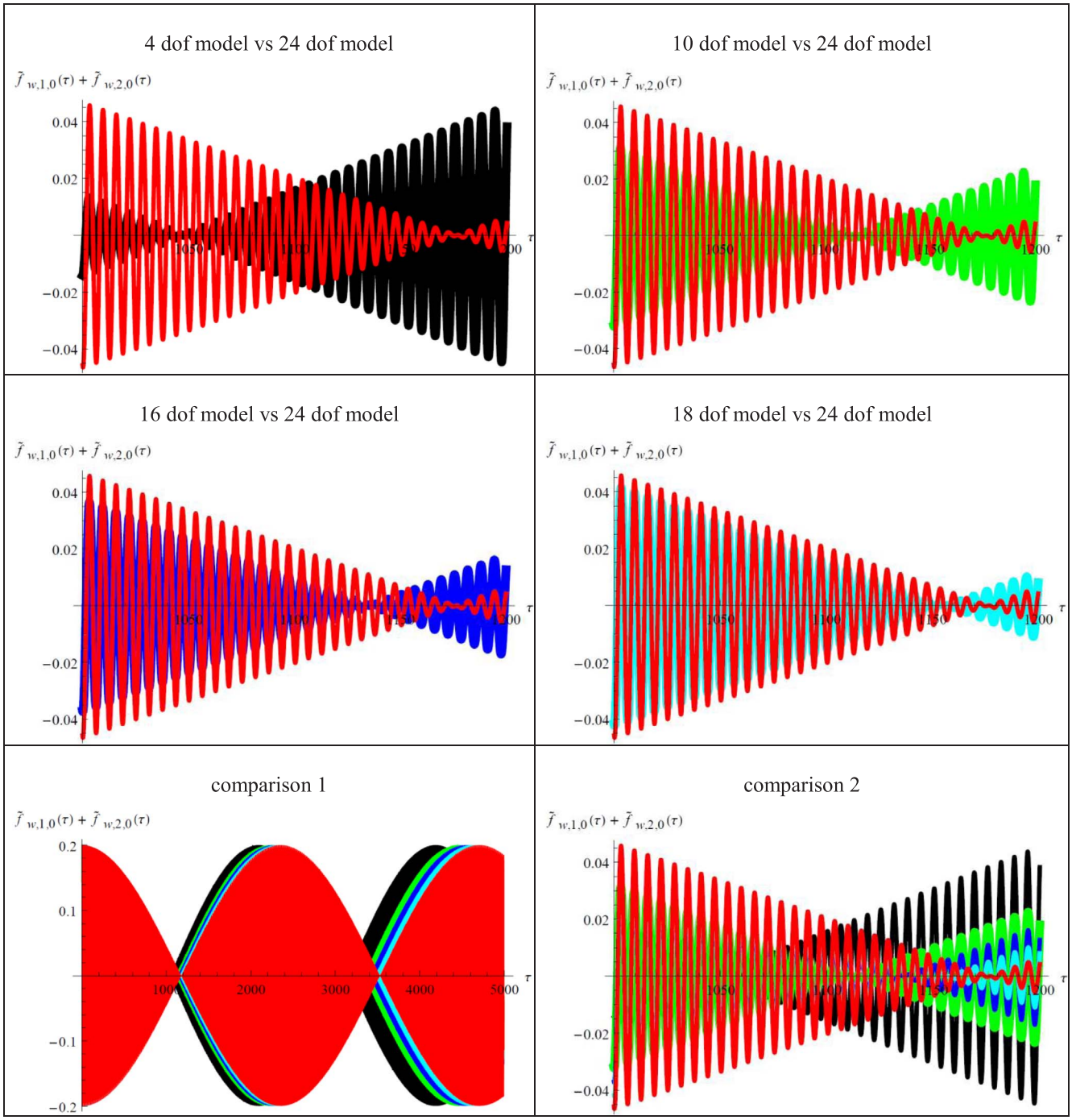

Fig. 4. Convergence analysis. Numerical method. Nonlinear modal expansions. Clamped-clamped edges. $L/R = 20$. Initial amplitude $\widetilde{X}(0) = 0.100$. Time histories. "—", 4 dof. "—", 10 dof. "—", 16 dof. "—", 18 dof. "—", 24 dof.

Table 6
Convergence analysis. Numerical method. Nonlinear modal expansions. Nonlinear energy beating period τ_b. Reference 24 dof model. Free-free edges. Aspect ratio $L/R = 20$. Initial excitation amplitude $\widetilde{X}(0) = 0.100$.

(j,n)	(1,0)	(2,0)	(3,0)	(1,2)	(2,2)	(3,2)	(1,4)	(2,4)	(3,4)	τ_b	$\Delta\tau_b$ %
4 dof model	*u, w*	*u, w*	–	–	–	–	–	–	–	2573	7.91
10 dof model	***u, w***	***u, w***	**–**	***u, v, w***	***u, v, w***	**–**	**–**	**–**	**–**	**2681**	**4.06**
16 dof model	*u, w*	*u, w*	–	*u, v, w*	*u, v, w*	–	*u, v, w*	*u, v, w*	–	2718	2.73
18 dof model	*u, w*	*u, w*	*u, w*	*u, v, w*	*u, v, w*	–	*u, v, w*	*u, v, w*	–	2754	1.44
24 dof model	*u, w*	*u, w*	*u, w*	*u, v, w*	*u, v, w*	*u, v, w*	*u, v, w*	*u, v, w*	*u, v, w*	2794	

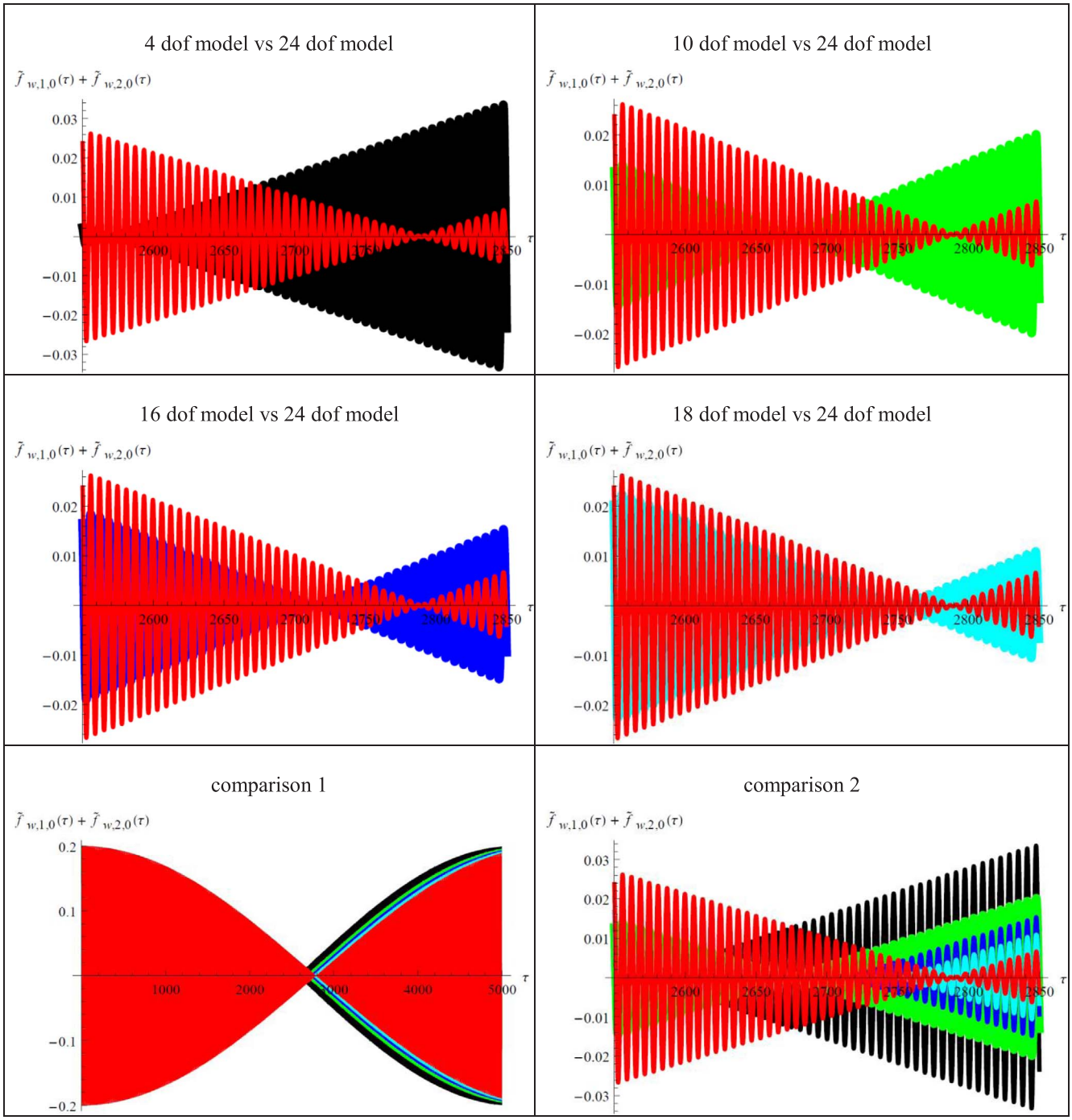

Fig. 5. Convergence analysis. Numerical method. Nonlinear modal expansions. Free-Free edges. $L/R = 20$. Initial amplitude $\widetilde{X}(0) = 0.100$. Time histories. "—", 4 dof. "—", 10 dof. "—", 16 dof. "—", 18 dof. "—", 24 dof.

histories of the 10 dof nonlinear modal expansions under different boundary conditions of Figs. 3–5 are given; the SWNT of Table 1 with aspect ratio $L/R = 20$ is considered; the initial excitation amplitude $\widetilde{X}(0) = 0.100$ is applied; the initial excitation domain ($\tau = 0$) is localized in the second half of the SWNT axis ($0.5 \leq \eta \leq 1$). From this comparison, it is confirmed that, for specific aspect ratio, initial excitation amplitude and nonlinear modal expansion, the nonlinear energy beating period τ_b depends on the applied boundary conditions; in particular, it assumes the lowest value for the clamped-clamped edges ($\tau_b = 1123$), the highest value for the free-free edges ($\tau_b = 2681$), and an intermediate value for the simply supported edges ($\tau_b = 2075$). In addition, it must be highlighted that, in the specific case of free-free boundary conditions, due to the particular mode shape of the modes (1,0) and (2,0), the energy is concentrated in the neighbourhood of the edges of the carbon nanotube axis (i.e., $\eta = 0$ or $\eta = 1$).

5.3. Nonlinear energy beating period

In this section, the effect of the aspect ratio L/R on the numerical value of the nonlinear energy beating period τ_b is investigated; the zigzag ($r = 20$, $s = 0$) SWNT of Table 1 is considered; the 10 dof nonlinear modal expansion given in the previous convergence analysis is applied; simply supported, clamped-clamped and free-free boundary conditions are analysed; the initial excitation amplitude $\widetilde{X}(0) = 0.100$ is

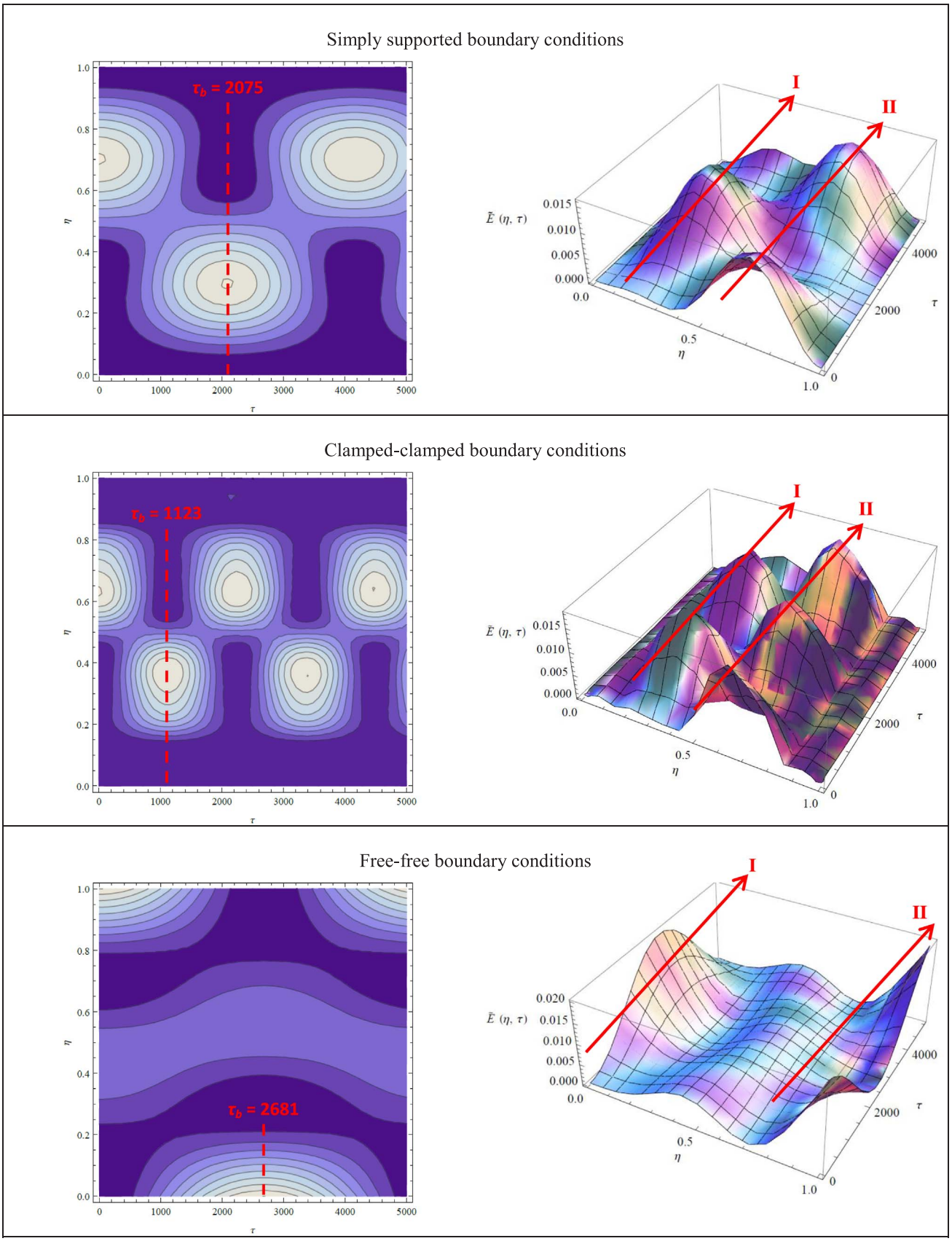

Fig. 6. Total energy distribution of the SWNT of Table 1 with aspect ratio $L/R = 20$ under different boundary conditions. Numerical method. 10 dof nonlinear modal expansion. Initial excitation amplitude $\widetilde{X}(0) = 0.100$.

Table 7
Nonlinear vibrations of the SWNT of Table 1. Numerical method. 10 dof nonlinear modal expansion. Initial excitation amplitude $\widetilde{X}(0) = 0.100$. Simply supported, clamped-clamped and free-free boundary conditions. Effect of the aspect ratio L/R on the value of the frequency parameter ε and the nonlinear energy beating period τ_b.

Aspect ratio	Boundary conditions		
	Simply supported edges	Clamped-clamped edges	Free-free edges
$L/R = 20$	$\varepsilon = 0.03890$ $\tau_b = 2075$	$\varepsilon = 0.05287$ $\tau_b = 1123$	$\varepsilon = 0.03422$ $\tau_b = 2681$
$L/R = 40$	$\varepsilon = 0.01856$ $\tau_b = 9120$	$\varepsilon = 0.02028$ $\tau_b = 7635$	$\varepsilon = 0.01674$ $\tau_b = 11200$
$L/R = 60$	$\varepsilon = 0.01233$ $\tau_b = 20650$	$\varepsilon = 0.01278$ $\tau_b = 19225$	$\varepsilon = 0.01112$ $\tau_b = 25390$
$L/R = 80$	$\varepsilon = 0.00910$ $\tau_b = 37920$	$\varepsilon = 0.00946$ $\tau_b = 35100$	$\varepsilon = 0.00832$ $\tau_b = 45340$
$L/R = 100$	$\varepsilon = 0.00733$ $\tau_b = 58440$	$\varepsilon = 0.00748$ $\tau_b = 56120$	$\varepsilon = 0.00666$ $\tau_b = 70820$

applied on the two resonant RBMs (1,0),(2,0); the initial excitation domain ($\tau = 0$) is imposed to be always localized in the second half of the SWNT axis ($0.5 \leq \eta \leq 1$).

From the numerical analyses for the RBM nonlinear vibrations reported in Table 7, it can be seen that, for a specific initial excitation amplitude and nonlinear modal expansion, the nonlinear energy beating period τ_b is dependent on the aspect ratio and boundary conditions considered; in particular, the beating parameter τ_b is inversely proportional to the squared frequency parameter ε, in the form

$$\tau_b = \frac{\pi}{\varepsilon^2} \qquad \varepsilon = \sqrt{\frac{\widetilde{\omega}_2 - \widetilde{\omega}_1}{\widetilde{\omega}_1}} \tag{30}$$

where ($\hat{\omega}_1$,$\hat{\omega}_2$) are the nondimensional circular frequencies of the radial breathing modes (1,0),(2,0), respectively.

From these comparisons, it can be seen that, for all the studied boundary conditions, the frequency parameter ε decreases and consequently the beating parameter τ_b increases by increasing the aspect ratio L/R (the difference between the circular frequencies of the first two RBMs reduces increasing the length of the carbon nanotube).

In particular, for each value of the aspect ratio, the free-free boundary conditions present the lowest frequency parameter ε and the highest beating parameter τ_b (slowest energy beating between the two halves of the SWNT axis); the clamped-clamped boundary conditions present the highest frequency parameter ε and the lowest beating parameter τ_b (fastest energy beating between the two halves of the SWNT axis); the simply supported boundary conditions are an intermediate case (intermedium value of the frequency ε and beating τ_b parameters).

In Figs. 7–9, the time histories and evolutions of the total energy distribution in the time along the axis of the SWNT of Table 1 are given; simply supported, clamped-clamped and free-free boundary conditions are considered, respectively; the effect of the aspect ratio L/R on the nonlinear energy beating period τ_b is analysed. From these figures, similarly to the numerical analyses of Table 7, it is confirmed that, for all the considered boundary conditions, increasing the aspect ratio increases the beating parameter τ_b and slows the energy beating between the two halves of the SWNT axis.

5.4. Radial breathing mode shapes

In Figs. 10–12, the first six RBM shapes of the zigzag ($r = 20$, $s = 0$) SWNT of Table 1 with aspect ratio $L/R = 20$ are reported; simply supported, clamped-clamped and free-free boundary conditions are applied, respectively.

In particular, it must be underlined that the axisymmetric mode ($j = 1$, $n = 0$) of the free-free boundary conditions (Fig. 12) corresponds to the Love's inextensional mode (one-half of the wave length), in which the middle surface of the circular cylindrical shell deforms without any stretching and the generators of the cylinder remain straight during the vibration, see Ref. [29] for more details on the inextensional theory of shells.

This graphical representation of the RBMs could be useful for properly interpreting the previous numerical results and comparisons of time histories and total energy distributions along the axis of the SWNTs.

6. Conclusions

In this paper, the nonlinear vibrations and energy exchange of SWNTs are studied. The Sanders-Koiter shell theory is applied to model the nonlinear dynamics of the system. Simply supported, clamped and free boundary conditions are considered. The RBMs are analysed. An energy method based on the Lagrange equations is used to obtain a set of nonlinear ordinary differential equations of motion, which is solved numerically by applying the implicit Runge-Kutta method.

This numerical model is validated in linear field by means of comparisons with data retrieved from the pertinent literature, i.e., resonant Raman spectroscopy and molecular dynamics simulations. The natural frequencies of the RBMs based on the numerical approach are in very good agreement with the experimental RRS and MDS results for several armchair, zigzag and chiral SWNTs under free-free boundary conditions, where the relative errors are less than 5%. Moreover, it is proved that the equivalent mechanical parameters of the SWNTs used in the present paper are correct, and the size effects do not affect significantly the RBM natural frequencies of the SWNTs considered.

In the second part of the paper, the energy exchange along the SWNT axis in the nonlinear field is investigated: imposing different initial excitation amplitudes on the two lowest frequency resonant RBMs of a simply supported SWNT with a specific aspect ratio, it is found that the initial localized energy is always immediately destroyed and a periodic energy exchange between the two halves of the SWNT axis takes place, where the nonlinear energy beating period τ_b is not dependent on the initial excitation amplitude (no nonlinear energy localization in one half of the SWNT axis).

A nonlinear convergence analysis is then carried out to select the correct number of axisymmetric and asymmetric modes providing the effective nonlinear behaviour of the SWNTs; different modal expansions and boundary conditions are used; a specific value of aspect ratio and initial excitation amplitude is considered; the 24 dof modal expansion is assumed as the reference model. For all the boundary conditions, all the considered models converge to a nonlinear behaviour similar to the 24 dof expansion; the 4 dof expansion (containing two axisymmetric modes) leads to the least accurate nonlinear behaviour; on the other hand, the 10 dof expansion (containing two axisymmetric modes and two asymmetric modes) denotes a nonlinear behaviour very close to the 24 dof expansion with minimal computational effort: therefore, this last modal expansion will be used in the calculations.

At the end, the influence of the aspect ratio on the value of the nonlinear energy beating period τ_b is investigated; the 10 dof nonlinear modal expansion is considered; different boundary conditions are evaluated; a specific value of initial excitation amplitude is applied. For all the boundary conditions, by increasing the aspect ratio increases the nonlinear energy beating period and therefore slows the energy exchange between the two halves along the SWNT axis. Moreover, for a specific value of aspect ratio, the free-free boundary conditions present the highest nonlinear energy beating period τ_b and the slowest energy exchange between the two halves along the SWNT axis, the clamped-clamped boundary conditions give the lowest nonlinear energy beating period and the fastest energy exchange between the two halves along the SWNT axis, the simply supported boundary conditions representing an intermediate case.

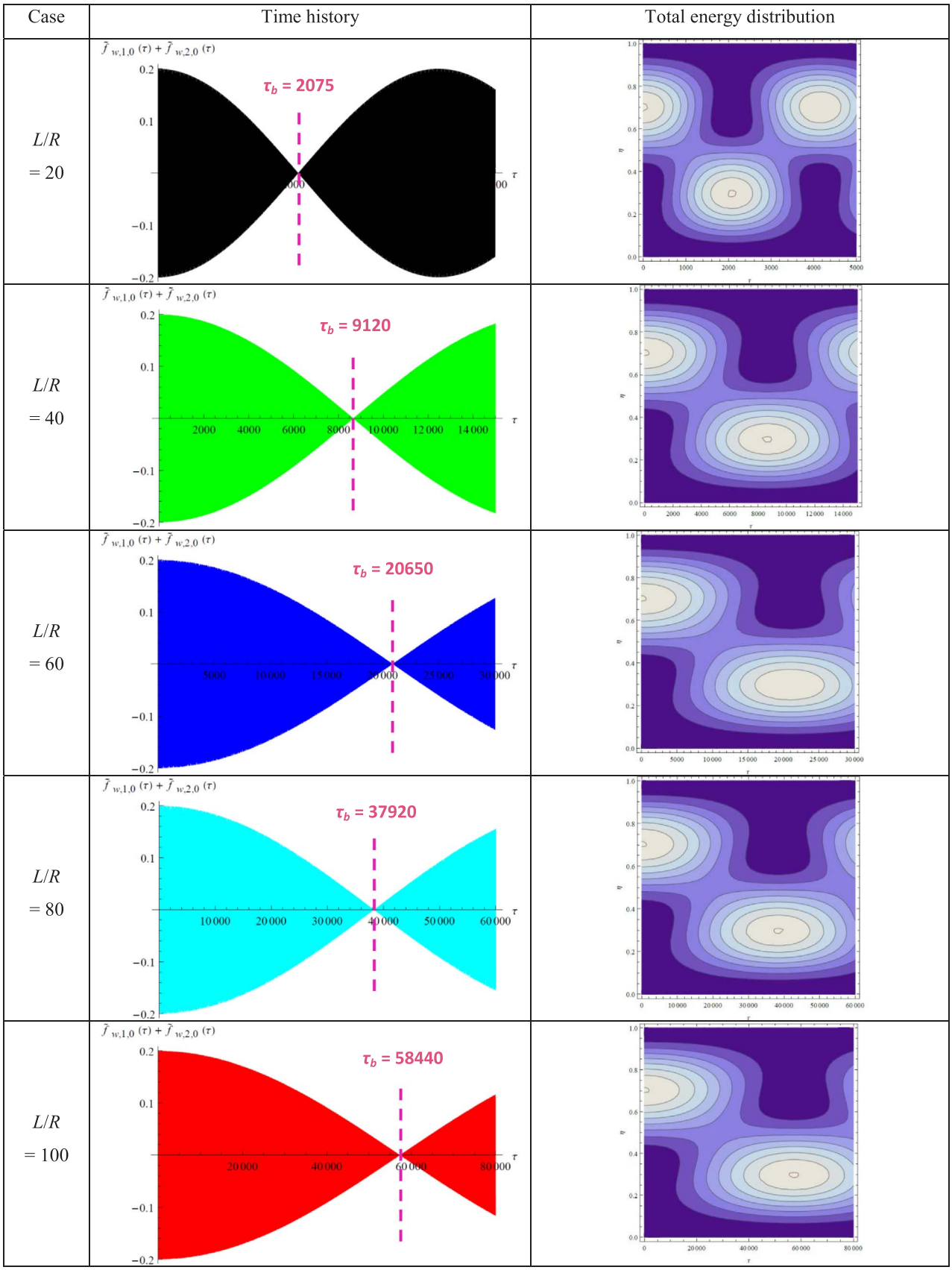

Fig. 7. Nonlinear vibrations of the simply supported SWNT of Table 1. Numerical method. 10 dof model. Initial excitation amplitude $\widetilde{X}(0) = 0.100$. Effect of the aspect ratio L/R on the nonlinear energy beating period τ_b.

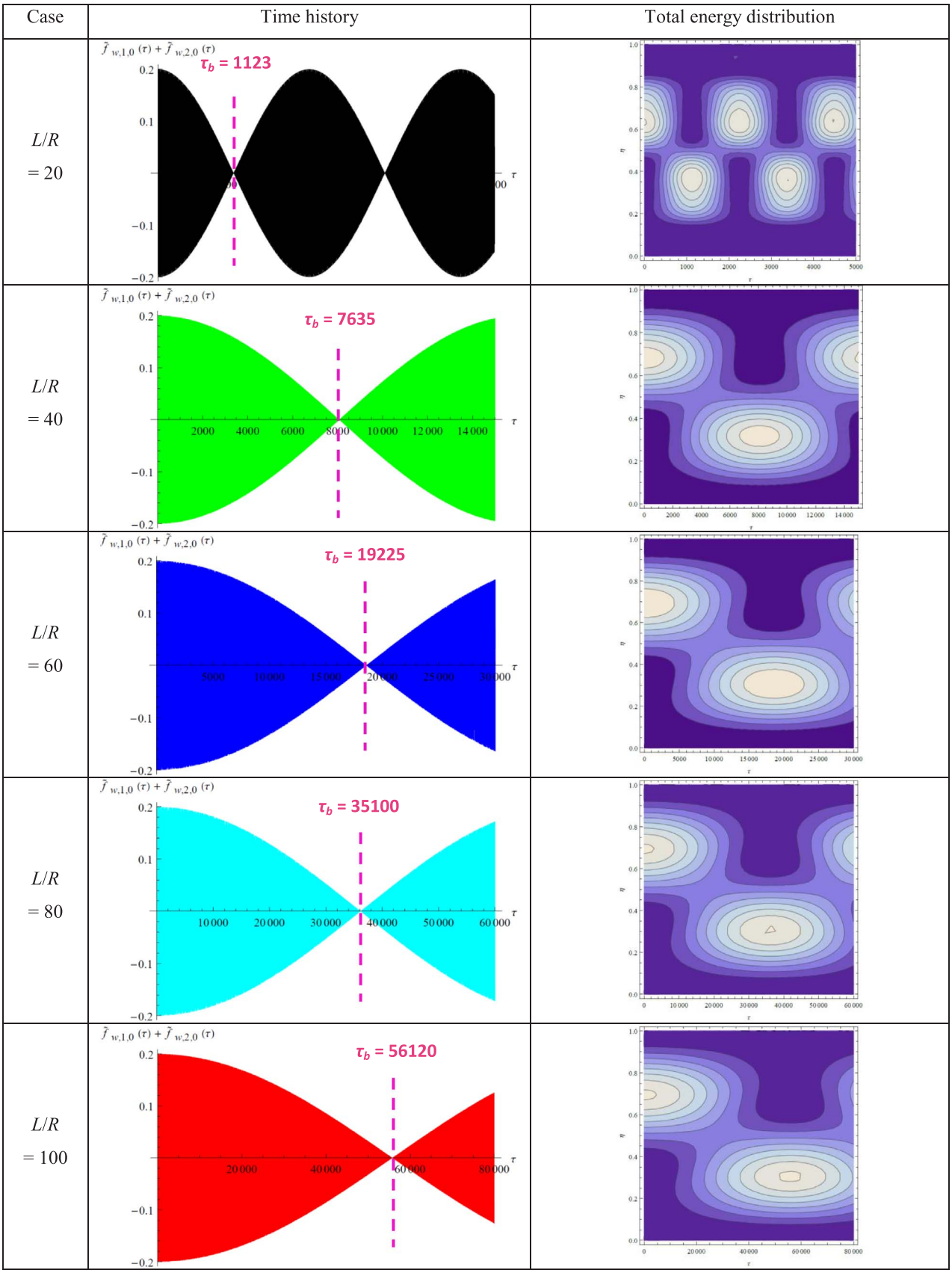

Fig. 8. Nonlinear vibrations of the clamped-clamped SWNT of Table 1. Numerical method. 10 dof model. Initial excitation amplitude $\widetilde{X}(0) = 0.100$. Effect of the aspect ratio L/R on the nonlinear energy beating period τ_b.

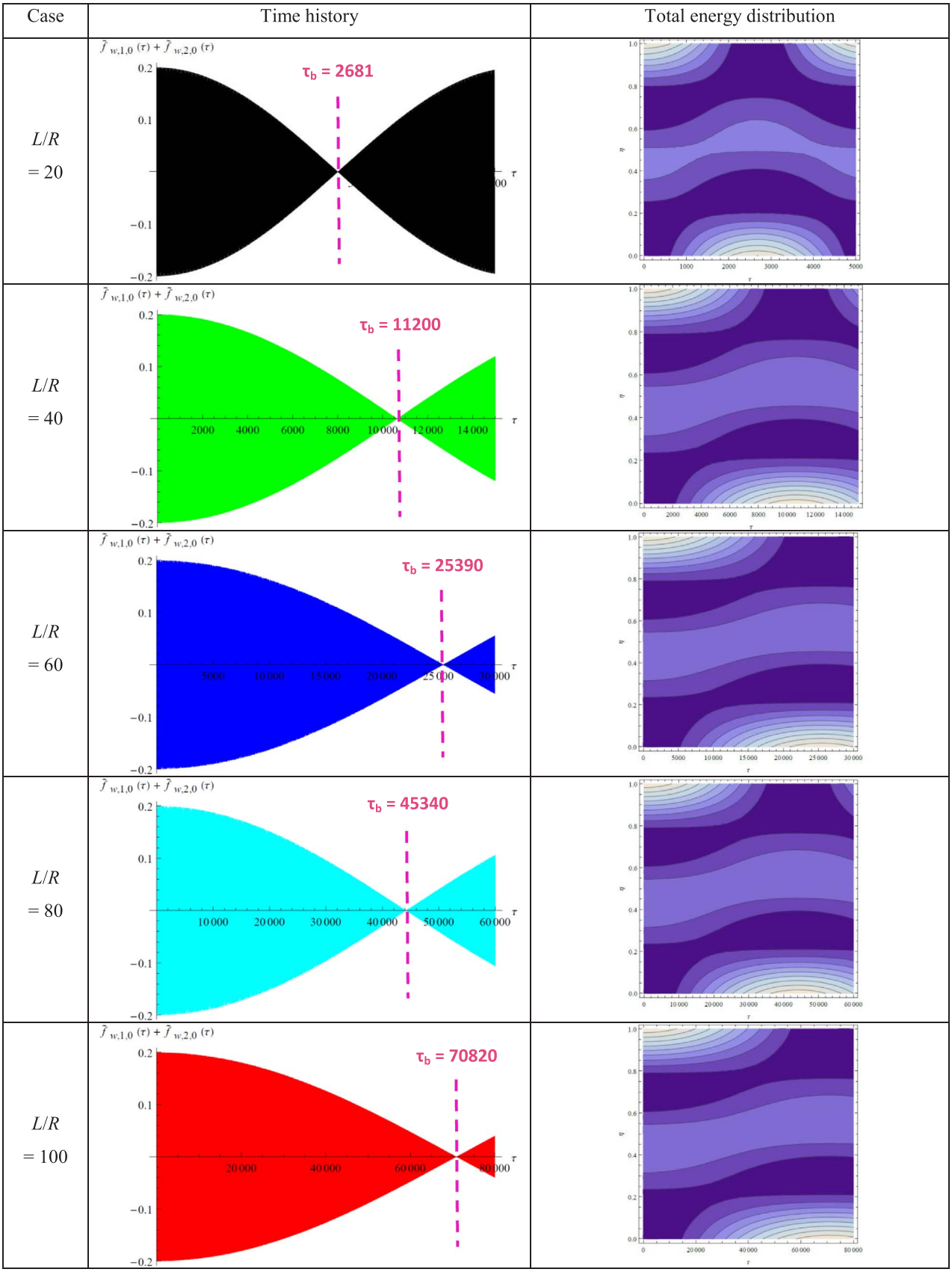

Fig. 9. Nonlinear vibrations of the free-free SWNT of Table 1. Numerical method. 10 dof model. Initial excitation amplitude $\widetilde{X}(0) = 0.100$. Effect of the aspect ratio L/R on the nonlinear energy beating period τ_b.

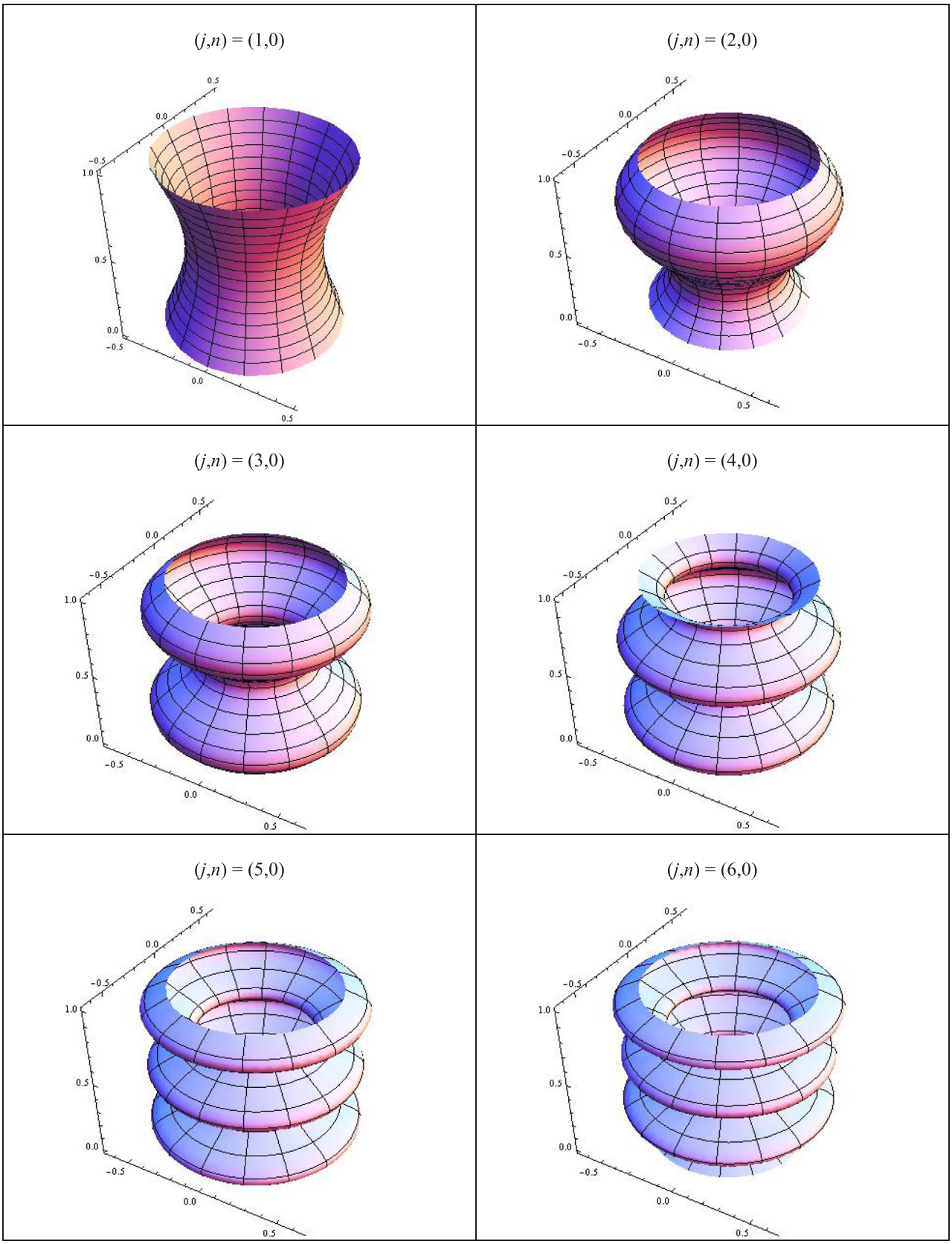

Fig. 10. RBM shapes of the SWNT of Table 1. Aspect ratio $L/R = 20$. Simply supported boundary conditions.

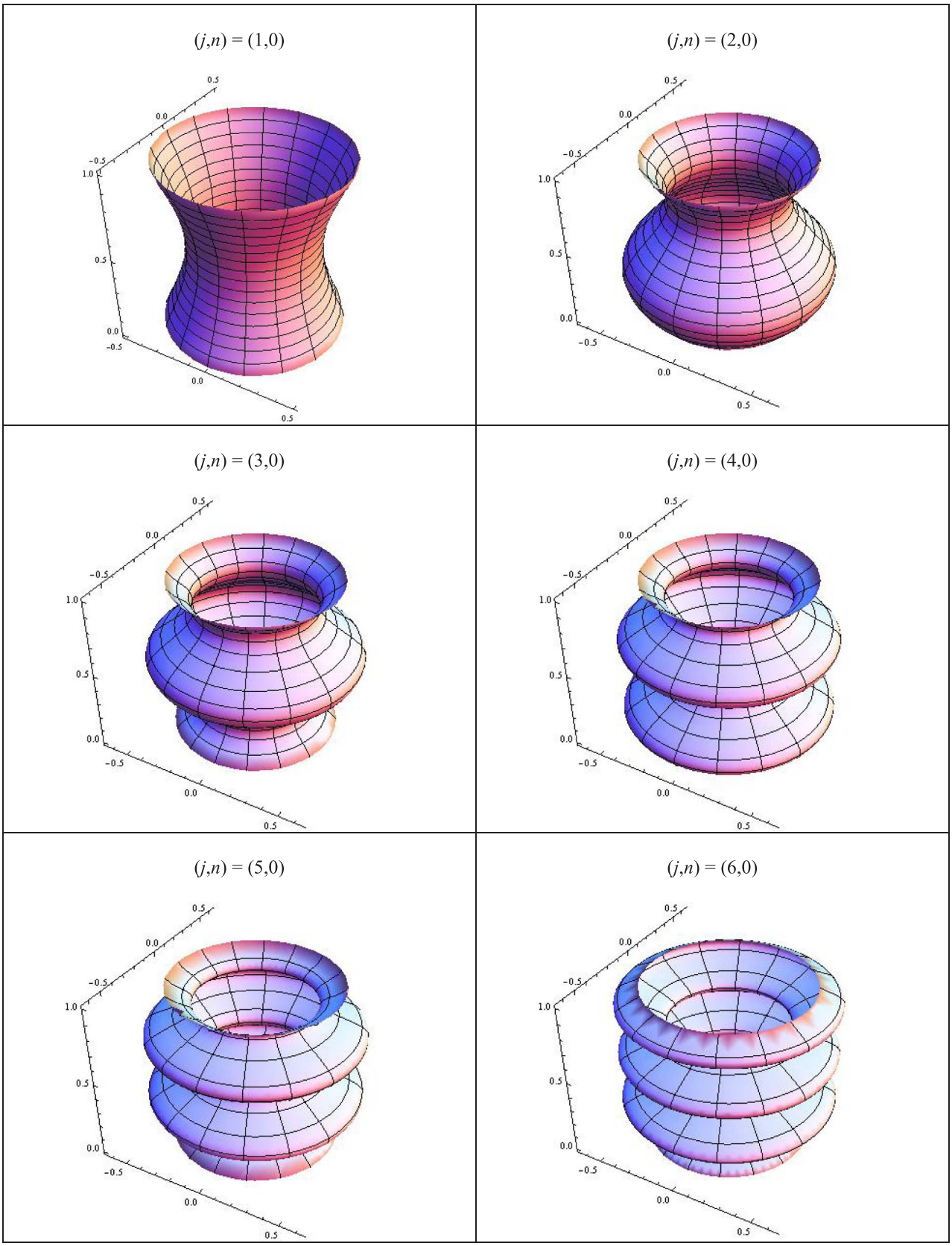

Fig. 11. RBM shapes of the SWNT of Table 1. Aspect ratio $L/R = 20$. Clamped-clamped boundary conditions.

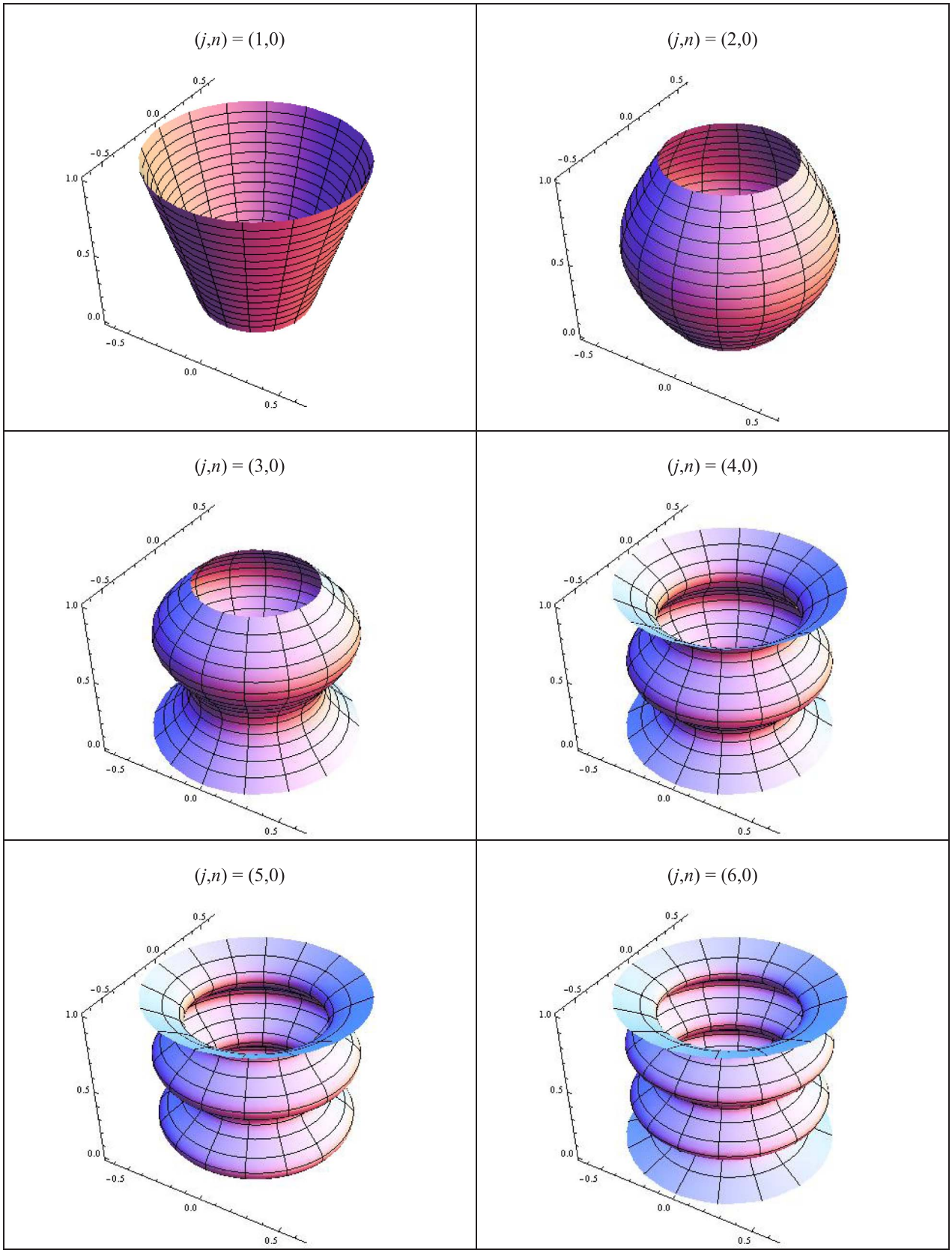

Fig. 12. RBM shapes of the SWNT of Table 1. Aspect ratio $L/R = 20$. Free-free boundary conditions. The axisymmetric mode ($j = 1$, $n = 0$) corresponds to the Love's inextensional mode (one-half of the wave length) [29].

6.1. Most relevant results achieved by the authors in the present study

The most relevant results on the energy exchange along the SWNT axis in nonlinear field achieved by the authors in the present paper focused on the nonlinear vibrations of RBMs, with regards to the results obtained by the same authors in the previous paper [26] devoted to the nonlinear vibrations of CFMs, are listed below.

- In the case of RBMs (differently from CFMs), the low-frequency nonlinear vibrations do not become localized ones forever in time for any amplitude of the initial excitation applied and no nonlinear energy localization in one half of the SWNT axis is achieved.
- By imposing different initial excitation amplitudes on the two lowest frequency resonant RBMs of a SWNT, it is found that the initial localized energy is immediately destroyed and a periodic energy exchange between the two halves of the SWNT axis takes place.
- From the numerical analyses for the RBM nonlinear vibrations, it is found that the nonlinear energy beating period does not depend on the initial excitation amplitude imposed, while it depends on the aspect ratio and boundary conditions considered.

Acknowledgments

Authors V.V. Smirnov and L.I. Manevitch are grateful to Russia Science Foundation (grant 16-13-10302) for the financial supporting of this work.

References

[1] Iijima S. Helical microtubules of graphitic carbon. Nature 1991;354:56–8.
[2] Dresselhaus MS, Dresselhaus G, Charlier JC, Hernandez E. Electronic, thermal and mechanical properties of carbon nanotubes. Philos Trans R Soc London A 2004;362:2065–98.
[3] Thostenson ET, Ren Z, Chou TW. Advances in the science and technology of carbon nanotubes and their composites. Compos Sci Technol 2001;61:1899–912.
[4] Gibson RF, Ayorinde EO, Wen YF. Vibrations of carbon nanotubes and their composites: a review. Compos Sci Technol 2007;67:1–28.
[5] Mahar B, Laslau C, Yip R, Sun Y. Development of carbon nanotube-based sensors. A review. IEEE Sens J 2007;7:266–84.
[6] Ouakad HM, Younis MI. Nonlinear dynamics of electrically actuated carbon nanotube resonators. J Comput Nonlinear Dyn 2010;5(13):011009.
[7] Li C, Thostenson ET, Chou TW. Sensors and actuators based on carbon nanotubes and their composites: a review. Compos Sci Technol 2008;68:1227–49.
[8] Hone J, Llaguno M, Biercuk MJ, Johnson AT, Batlogg B, Benes Z. Thermal properties of carbon nanotubes and nanotube-based materials. Appl Phys A 2002;74:339–43.
[9] Han Z, Fina A. Thermal conductivity of carbon nanotubes and their polymer nanocomposites: a review. Prog Polym Sci 2011;36:914–44.
[10] Manevitch LI, Gendelman OV. Tractable models of solid mechanics. Formulation, analysis and interpretation. Berlin: Springer-Verlag; 2011.
[11] Rao AM, Richter E, Bandow S, Chase B, Eklund PC, Williams KA, et al. Diameter-selective Raman scattering from vibrational modes in carbon nanotubes. Science 1997;275:187–91.
[12] Jorio A, Saito R, Hafner JH, Lieber CM, Hunter M, McClure T, et al. Structural (n, m) determination of isolated single-wall carbon nanotubes by resonant Raman scattering. Phys Rev Lett 2001;86:1118–21.
[13] Araujo PT, Pesce PBC, Dresselhaus MS, Sato K, Saito R, Jorio A. Resonance Raman spectroscopy of the radial breathing modes in carbon nanotubes. Physica E 2010;42:1251–61.
[14] Gupta SS, Bosco FG, Batra RC. Breakdown of structural models for vibrations of single-wall zigzag carbon nanotubes. J Appl Phys 2009;106(9):063527.
[15] Cheng HC, Liu YL, Wu CH, Chen WH. On radial breathing vibration of carbon nanotubes. Comput Methods Appl Mech Eng 2010;199:2820–7.
[16] Gupta SS, Bosco FG, Batra RC. Wall thickness and elastic moduli of single-walled carbon nanotubes. Comput Mater Sci 2010;47:1049–59.
[17] Batra RC, Gupta SS. Wall thickness and radial breathing modes of single-walled carbon nanotubes. J Appl Mech 2008;75(6):061010.
[18] He XQ, Eisenberger M, Liew KM. The effect of van der Waals interaction modelling on the vibrations of multi-walled carbon nanotubes. J Appl Phys 2006;100(12):124317.
[19] Elishakoff I, Pentaras D. Fundamental natural frequencies of double walled carbon nanotubes. J Sound Vib 2009;322:652–64.
[20] Liew KM, Wang Q. Analysis of wave propagation in carbon nanotubes via elastic shell theories. Int J Eng Sci 2007;45:227–41.
[21] Silvestre N, Wang CM, Zhang YY, Xiang Y. Sanders shell model for buckling of single-walled carbon nanotubes with small aspect ratio. Compos Struct 2011;93:1683–91.
[22] Strozzi M, Manevitch LI, Pellicano F, Smirnov VV, Shepelev DS. Low-frequency linear vibrations of single-walled carbon nanotubes: analytical and numerical models. J Sound Vib 2014;333:2936–57.
[23] Manevitch LI, Smirnov VV, Strozzi M, Pellicano F. Nonlinear optical vibrations of single-walled carbon nanotubes. Int J Non-Linear Mech 2017;94:351–61.
[24] Peng J, Wu J, Hwang KC, Song J, Huang Y. Can a single-wall carbon nanotube be modeled as a thin shell? J Mech Phys Solids 2008;56:2213–24.
[25] Fazelzadeh SA, Ghavanloo E. Nonlocal anisotropic elastic shell model for vibrations of single-walled carbon nanotubes with arbitrary chirality. Compos Struct 2012;94:1016–22.
[26] Strozzi M, Smirnov VV, Manevitch LI, Milani M, Pellicano F. Nonlinear vibrations and energy exchange of single-walled carbon nanotubes. Circumferential flexural modes. J Sound Vib 2016;381:156–78.
[27] Yakobson BI, Brabec CJ, Bernholc J. Nanomechanics of carbon tubes: instabilities beyond linear response. Phys Rev Lett 1996;76:2511–4.
[28] Wang L, Zheng Q, Liu JZ, Jiang Q. Size dependence of the thin-shell model for carbon nanotubes. Phys Rev Lett 2005;95(4):105501.
[29] Leissa AW. Vibrations of shells. Washington, DC: Government Printing Office; 1973.
[30] Yamaki N. Elastic stability of circular cylindrical shells. Amsterdam: North-Holland; 1984.